Single- and mixed-gas sorption in large-scale molecular models of glassy bulk polymers. Competitive sorption of a binary CH4/N2 and a ternary CH4/N2/CO2 mixture in a polyimide membrane

Sylvie Neyertz, David Brown

Single- and Mixed-Gas Sorption in Large-Scale Molecular Models of Glassy Bulk Polymers. Competitive Sorption of a Binary CH_4/N_2 and a Ternary $CH_4/N_2/CO_2$ Mixture in a Polyimide Membrane

Sylvie NEYERTZ* and David BROWN

Univ. Savoie Mont Blanc, Univ. Grenoble Alpes, CNRS, Grenoble INP, LEPMI, 38000 Grenoble, France

*Corresponding author: Sylvie.Neyertz@univ-smb.fr, postal address: LEPMI, CNRS UMR 5279, Univ. Savoie Mont Blanc, Bât. Hélios, Savoie Technolac, 73376 Le Bourget du Lac Cedex, France

Tel: +33 4 79758697

GRAPHICAL ABSTRACT

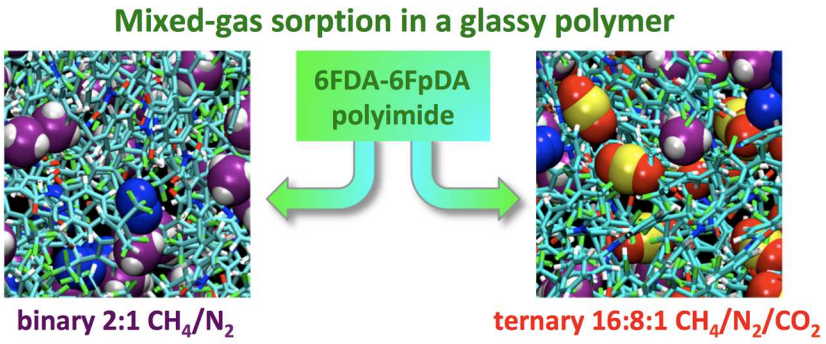

ABSTRACT

Three molecular simulation techniques to predict the gas sorption isotherms in a glassy polymer membrane in contact with a single- or a mixed-gas reservoir have been tested on a large-scale ~50000 atom 6FDA-6FpDA polyimide bulk model over a wide range of pressures. Both single- and mixed-gas uptake curves were obtained for CH_4, N_2 and CO_2 over the 0-60 bar range using either a Grand Canonical Monte Carlo (GCMC), an iterative test particle insertion - molecular dynamics (TPI-MD) or an iterative GCMC-MD method. Virtual TPI and actual GCMC insertions of gas molecules into the polymer matrices were performed using the excluded-volume map sampling approach (EVMS), which improved the sampling efficiencies by a factor of ~10-20 over random insertions.

The simulation techniques were first used to obtain the single-gas sorption isotherms and the associated ideal gas sorption selectivities. The TPI-MD and GCMC-MD approaches gave consistent results in agreement with experiment. Further tests were made on a binary 2:1 CH_4/N_2 and a ternary 16:8:1 $CH_4/N_2/CO_2$ gas mixture in equilibrium with the 6FDA-6FpDA model matrix. For such mixed-gas feeds, the uptake of each gas in the polymer depends on its gas phase concentration and on its solubility in both the gas mixture and the polymer phases. Solubilities of penetrants in the polymer phase correlated well to the total penetrant concentration. In the binary mixture, the sorption of N_2 was strongly hindered by that of CH_4. In the ternary mixture, the introduction of the highly-soluble CO_2 at a relatively low partial pressure significantly reduced the sorption of both CH_4 and N_2, although its concentration was insufficient to plasticize the polymer. As such, the mixed-gas CH_4/N_2, CO_2/CH_4 and CO_2/N_2 sorption selectivities were found to differ from their ideal values. Interference effects were characterized by a novel technique which estimates the proportions of molecules of each type of penetrant excluded by competitive sorption for the mixtures under study.

The main asset of such iterative molecular simulations is their ability to take implicitly into account the interdependence of the different gas concentrations and solubilities as well as the associated changes in the matrices over a large range of pressures and temperatures. In addition, the iterative GCMC-MD method should be applicable to even more complex mixtures, which is obviously pertinent with respect to industrial gas separation applications.

Keywords: Grand Canonical Monte Carlo (GCMC), iterative test particle insertion - molecular dynamics (TPI-MD), iterative GCMC-MD, glassy polymer membranes, gas sorption, single-gas, mixed-gas, binary and ternary gas mixtures

I. INTRODUCTION

Separations of mixtures are critical when they involve molecules of a similar size, *e.g.* small gases. Traditional processes used in gas separations such as cryogenic distillation are very energy-intensive and require large investments and operating costs. On the other hand, dense polymer membranes are growing in use as a cost-effective, flexible and easy-to-scale-up alternative due to their ability to separate small gas molecules based on differences in gas diffusivities and solubilities [1, 2]. For separation of well-known gases such as N_2, CH_4 and CO_2, polymers are more efficient when they are in the glassy state, *i.e.* below their glass transition temperature T_g [3]. Transport occurs via the solution-diffusion mechanism [4, 5], in which gas molecules in an upstream reservoir are absorbed into the membrane, diffuse through the dense matrix and eventually desorb into a downstream reservoir. Gas permeability P_{gas} can be obtained from the diffusion and solubility coefficients with $P_{gas} = D_{gas} \times S_{gas}$. In the presence of two gas components A and B, the ideal permselectivity $\alpha_{A/B}$ (also called separation factor) of the membrane is the ratio of the pure permeabilities of both gases:

$$\alpha_{A/B} = \frac{P_A}{P_B} = \left(\frac{D_A}{D_B}\right) \times \left(\frac{S_A}{S_B}\right) = \alpha^D_{A/B} \times \alpha^S_{A/B} \quad (1)$$

with $\alpha^D_{A/B}$ and $\alpha^S_{A/B}$ being the diffusion and the solubility (or sorption) selectivities, respectively. Eq. (1) is well adapted when low-solubility gases are involved, *e.g.* in the case of air separation (O_2/N_2) [6], but it is a lot less accurate when at least one of the penetrants interacts strongly with either the polymer matrix and/or the other penetrants [1]. This is illustrated by natural gas sweetening (CO_2/CH_4) or nitrogen extraction (N_2/CH_4), in which the actual separation factor $\alpha^*_{A/B}$ differs from the ideal permselectivity [7-11]. While most experimental and model membrane studies are performed for convenience with pure gases and their performances are evaluated using Eq. (1), there is an increasing need to characterize the relevant materials under conditions which are much closer to the operating processes. These include mixed-gas reservoirs under a wide range of compositions, pressures and temperatures [8, 9, 12-14]. Within this context, models should be able to complement the difficult and time-consuming measurements by predicting the gas uptakes under a large variety of operating conditions [9].

Unfortunately, modelling mixed-gas sorption in glassy polymer matrices is far from being straightforward [14, 15]. There have been significant contributions using the dual-mode sorption (DMS) model [14, 16, 17], the non-equilibrium thermodynamics of glassy polymers (NET-GP) approach [13, 18-22] or other theories [23, 24]. Alternatively, molecular simulations including molecular dynamics (MD) and Monte Carlo (MC) approaches can also be used. Molecular models are clearly time- and resource-consuming, but they provide structural and dynamical information at the atomistic level, which can help towards the design of structures with better performances. In addition, once the model polymer matrix has been validated, it can be re-used to screen different separations under a large variety of operating conditions. Several specific methodologies have been developed to address the penetrant solubility/diffusion/permeation processes in glassy polymers and they are exposed in a recent review [15]. Most of them apply to bulk models, which represent the membrane cores and, as such, are associated to the limiting values of the transport parameters.

In bulk molecular models, periodicity in three dimensions is applied to the primary simulation box in order to avoid edge-effects related to their limited sizes, *i.e.* typically a few cubic nanometers. The disadvantage is that there are no explicit reservoirs in contact with the polymer sample. This is problematic when one attempts to simulate the uptake of a gas since, to be consistent with the experimental set-up, the number of gas molecules absorbed into the polymer model should be dependent on the external gas pressure. Grand Canonical Monte Carlo (GCMC) [25] is currently the most commonly-used technique to model gas sorption in pre-prepared bulk models [23, 26-28]. It allows for the polymer to exchange gas molecules with an infinite virtual gas bath until the equilibrium penetrant concentration is reached within the matrix. However, a basic assumption of GCMC is that the matrix configurations are static, *i.e.* the volume is constant. This can lead to artefacts, especially when plasticizing penetrants are present [28, 29]. On the other hand, MD allows naturally for the matrix to change, *e.g.* through dilation upon gas sorption. Van der Vegt et al. [30] have developed an iterative method for single-gas sorption based on the Test Particle Insertion (TPI) approach [31, 32] combined with MD, which estimates the pressure of an external gas reservoir in equilibrium with a fixed number of penetrant gas molecules inserted into the matrix. The MD simulation boxes are allowed to change shape and size at controlled pressure and the gas solubility in the polymer phase is evaluated from TPI post-processing calculations on the

stored MD configurations. The pressure is iterated until convergence is achieved. This specific technique, which we refer to as the "iterative pressure TPI-MD method" (iterative *p*-TPI-MD), has been successfully applied to the sorption of single-gases in several polyimides over large pressure ranges, *i.e.* up to 60 bar [33-35]. This is typically the upper limit of industrial interest for adsorption-based gas separations [36]. The TPI-MD approach has also been tested for a binary mixture [34], but in that case, the pressure was fixed and the numbers of both types of penetrants were changed until convergence; we refer to this specific adaptation as the "iterative number TPI-MD method" (iterative *n*-TPI-MD). Other approaches combine both Monte Carlo and molecular dynamics techniques [15, 37, 38]. For example, GCMC can be used to predict the number of sorbed gas molecules in a set of static configurations in equilibrium with a fictive reservoir held at a certain pressure, while controlled-pressure MD relaxes the model volume following the loading of the penetrant. Since the volume changes during the MD relaxation phase, several alternating cycles of GCMC and MD are usually necessary to reach convergence. This technique, which has been called the "sorption-relaxation approach", has also already been used to study the sorption of single-gases and binary mixtures in polyimides and copolyimides [39-42] or in PIM [28, 29]. We will refer to it here as the "iterative GCMC-MD method" in order to emphasize its cyclic character associated with the relaxation of the polymer matrix.

The aim of the present work is to apply all three aforementioned approaches, *i.e.* the GCMC on its own, the iterative TPI-MD and the iterative GCMC-MD, to both single-gas and mixed-gas sorption in a very large-scale glassy polymer bulk model, *i.e.* n_{atoms} ~50000. System sizes reported before typically range between n_{atoms} ~3000-6000 [20, 23, 26, 28, 29, 39-41] and n_{atoms} ~10000-15000 [33, 34, 38, 42], although the statistics can be significantly improved by averaging over several simulation boxes of the same size [20, 23, 28, 29, 33, 38]. Indeed, averages over eight models of ~(35 Å)^3 showed similar performances for helium permeation to those of a larger ~(85 Å)^3 model in a study of system-size dependence in polyimide models [43]. However, it is obviously at the expense of non-negligible standard deviations. The choice of a large system containing 15 chains of 50 monomers (~50000 atoms) stems from our former experience with single-gas CO_2 sorption in 6FDA-based polyimides, in which averages were made over three 3-chain systems (~10000 atoms) [33]. As will be shown in Section 3.2., reliable results for the gas

uptakes were difficult to obtain at high loadings from a single 3-chain system due to the variability in the solubility of the penetrant. A larger simulation box removes the need to average over different systems and it permits a better resolution to be obtained in terms of penetrant concentrations (since only integer changes in the number of molecules can be made). In addition, it reduces any possible system size-effects due to the polymer chains in these amorphous systems inevitably interacting with images of themselves through the periodic boundary conditions.

Larger model sizes result naturally in an increased need for computer resources, which can rapidly become prohibitive even on parallel processors. For example, the time needed to evaluate long-range electrostatic interactions typically scales as $n_{atoms}^{3/2}$ [44]. Although a polyimide model without partial charges has been reported [42], electrostatic interactions in O- , F- and N-containing polymers should not be neglected [45, 46]. To further improve the efficiency of the GCMC procedure, the attempted insertions of gas molecules into the polymer matrix were performed using the excluded-volume map sampling approach (EVMS) [47-49], which screens out polymer regions of very low insertion probabilities. EVMS had been previously included in the iterative TPI-MD procedure [33, 34]. In addition to a binary mixture, another contribution of the present study is the sorption isotherm of a ternary gas mixture in a glassy polymer which, to our knowledge, has not been attempted for atomistic models before. Furthermore, we introduce a procedure to characterize interference by evaluating the number of molecules of each type of gas excluded by competitive sorption for the mixtures under study.

The 6FDA-6FpDA polyimide (Fig. 1a) was chosen as a test case since many different groups have studied its properties [50-64]. A large-scale molecular model was prepared at 308 K in order to have a realistic representation of the membrane core. Details related to the glassy matrix are summarized in Section 2. Section 3 describes the optimized methodologies for single-gas sorption, including the introduction of the EVMS formalism into the GCMC sampling procedure. It also provides the single-gas uptake isotherms for CH_4, N_2 and CO_2 in 6FDA-6FpDA. Section 4 presents the adaptations to model mixed-gas sorption. Uptake curves are obtained over the 0-60 bar range when the 6FDA-6FpDA membrane is either in equilibrium with a 2:1 CH_4/N_2 binary-gas or with a 16:8:1 $CH_4/N_2/CO_2$ ternary-gas feed, both reservoirs being consistent with the composition of natural gas [9, 65]. We show that the optimized iterative methods can directly predict the

proportions of each penetrant within the glassy matrix under mixed-gas conditions. Furthermore, the iterative GCMC-MD can in principle be applied to even more complicated mixtures than binary or ternary feeds.

2. THE GLASSY POLYMER MATRIX

The force-field and the generation procedure for the bulk 6FDA-6FpDA model have already been described in details elsewhere [33, 66, 67]. Its degree of polymerization (DP), n = 50 monomers, is consistent with experiment [68]. With 15 chains and a total number of 49530 atoms (*i.e.* much larger than typical MD boxes used for fully-atomistic bulk systems [20, 23, 26, 29, 34, 38-42]), size-dependent effects should be small.

All simulations were carried out using the parallelized *gmq* package [69], which has good scaling properties [70]. The force-field was described by "bonded" potentials (angle-bending deformations, torsional motions and out-of-plane terms) arising from near-neighbour connections, and "non-bonded" potentials (van der Waals and electrostatic) depending on the distance between two interacting sites. The latter were calculated between atoms belonging either to the same chain and separated by more than two bonds or between atoms belonging to different molecules. To ensure equipartition of the kinetic energy, all bond stretching modes were removed using rigid bond constraints and the two remaining degrees of freedom of hydrogens in each C-H group were removed using special constraints [71, 72]. The implementation of such constraints allows for the use of a timestep larger than would be possible if these degrees of freedom were retained (for the same level of fluctuations in the total energy relative to the total potential energy) under *NVE* conditions (constant number of atoms N, constant volume V, constant energy E) conditions (see Fig. S1, Supp. Info.). In the present case, the fluctuations in the total energy were 0.75% with a timestep of 1 fs and over 3.3% with a timestep of 2 fs. As such, a timestep of 1 fs was chosen to integrate the equations of motion. Due to its long-range nature, the electrostatic potential was calculated using the Ewald summation method with (α, K_{max}) parameters equal to (0.22, 13) [73]. The other non-bonded cutoffs were set to 12 Å. Potential parameters have been given elsewhere [66].

Due to the timescales currently spanned by explicit-atom MD (~10^{-9} to 10^{-7} s for large molecules), the starting structures for amorphous polymers must already be relaxed prior to the MD

simulation. While several approaches are possible [74], we used the hybrid pivot Monte Carlo molecular dynamics single-chain procedure (PMC-MD), which generates chain configurations characteristic of the equilibrium melt at a required temperature [75]. In PMC-MD, the configurational phase-space of the chains is sampled using the pivot Monte Carlo moves [76] for rotatable torsions, while the MD algorithms explore the various oscillatory modes. The temperature T is kept to the required value by loose-coupling to a heat bath [77]. Decorrelation from the initial structures usually occur within a few thousand pivot moves. This approach has already been validated for 6FDA-6FpDA [66, 75]. Its sampling temperature was set at 650 K, *i.e.* just above the experimental T_g range [66], to ensure that the selected configurations are close to those expected for the glass. The melt was first relaxed under *NVT* conditions (constant volume V and controlled temperature T) and then cooled down to 308 K (35°C) at a rate of -1 K ps^{-1}. It was switched to ***NPT*** conditions (controlled pressure tensor $\boldsymbol{P}$ instead of V), in which the box is allowed to relax towards its equilibrium shape and size. The pressure was maintained close to 1 bar by loose-coupling [78]. We note that imposing a cubic box shape on a relatively small sample (by macroscopic standards) of a dense glassy polymer is tantamount to applying a complex pressure field to the system. On the other hand, ***NPT*** conditions allow for the on-diagonal components of the pressure tensor to relax to the imposed isostatic pressure and for the off-diagonal components to relax to zero, *i.e.* all box lengths and box angles can vary. The run continued under ***NPT*** conditions at 308 K for 9000 ps until all properties were stabilized. Under these conditions, the density settled to 1488.6±0.3 kg m^{-3}, *i.e.* within less than 1% of the average experimental value of 1475±4 kg m^{-3} [50-52, 54-57, 59-61, 63, 64]. Lyulin and coworkers have reported a small density dependence on the MD cooling rate for several polyimides [45, 46, 79]. Here, the density settles to 1486.3±0.2 kg m^{-3} with a higher cooling rate of -10 K ps^{-1}, which is only slightly lower than the value obtained with -1 K ps^{-1}. With the latter, the average relaxed cell lengths and angles were found to be $a = 85.06\pm0.02$ Å, $b = 86.04\pm0.01$ Å, $c = 84.90\pm0.02$ Å, $\alpha = 90.28°\pm0.02°$, $\beta = 89.09°\pm0.01°$ and $\gamma = 89.13\pm0.02°$. In addition, analyses of the configurations, stored every 20 ps during the simulation, were consistent with the average radius of gyration and characteristic ratio of 50-monomer 6FDA-6FpDA chains that have been reported recently [80]. A schematic representation of the 6FDA-6FpDA bulk

polymer displayed with the VMD (Visual Molecular Dynamics) software [81] is provided in Fig. 1b.

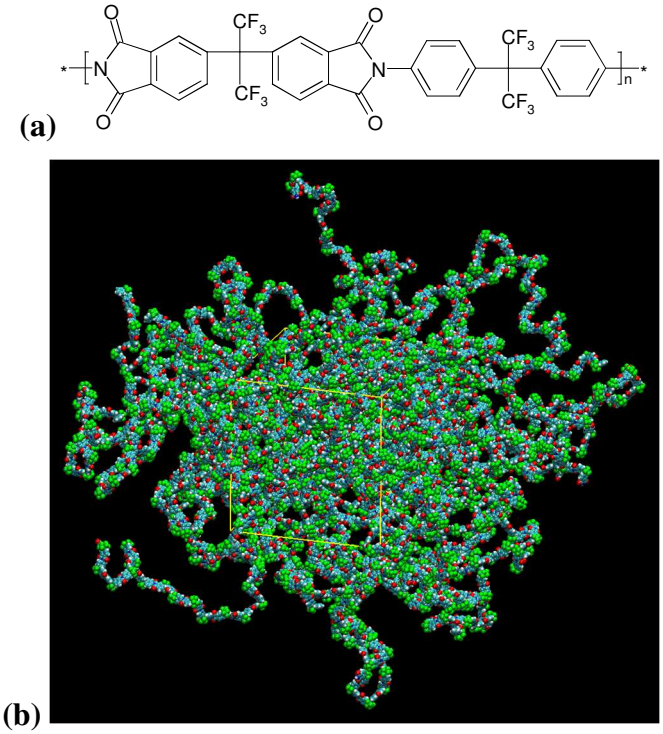

Fig. 1. **(a)** Chemical structure of the 6FDA-6FpDA polyimide, with *n* being here equal to 50. **(b)** The 49530-atom bulk model in its unfolded primary coordinates. Each atom situated outside of the simulation box has an image inside through the periodic boundary conditions. The colour code is: cyan = C, red = O, blue = N, white = H, green = F.

3. SINGLE-GAS SORPTION IN POLYMERS

3.1. Methodology

3.1.1. The test-particle insertion (TPI) technique

The solubility S of a gas molecule dissolved into a polymer matrix is linked to its excess free energy ΔG, the Boltzmann constant k_B and the temperature T [31]:

$$S = \exp\left(-\frac{\Delta G}{k_B T}\right) \tag{2}$$

In atomistic simulations, the free energy for the solvation process is usually estimated using the test-particle insertion (TPI) approach, in which a penetrant molecule is virtually inserted at random

sites into the matrix of volume V and the change in potential energy $\Delta\Phi$ associated with the insertion is calculated [31, 32]. We note that particle deletion schemes can also be used as an alternative [37, 82, 83]. In the case of TPI as applied to dense polymers, many millions of particle insertions have to be made in order to obtain converged averages. The excess chemical potential of the gas in the polymer, μ^{ex}, is given by the following equation [44]:

$$\mu^{ex} = -k_B T \ln \frac{\left\langle V \exp\left(-\frac{\Delta\Phi}{k_B T}\right)\right\rangle}{\langle V \rangle} \tag{3}$$

The (dimensionless) solubility S is then obtained by:

$$S = \exp\left(\frac{-\mu^{ex}}{k_B T}\right) = \frac{\left\langle V \exp\left(-\frac{\Delta\Phi}{k_B T}\right)\right\rangle}{\langle V \rangle} \approx \left\langle \exp\left(-\frac{\Delta\Phi}{k_B T}\right)\right\rangle \tag{4}$$

The right-hand approximation in Eq. (4) holds for materials where volume fluctuations are small, such as glassy polymers. An ideal gas has an $S = 1$ due to the absence of interactions. To improve its efficiency, the TPI method incorporated into *gmq* was parallelized and combined with an excluded-volume map sampling (EVMS), which screens out regions of very low insertion probabilities [47-49]. As already shown for the iterative TPI-MD approach [33, 34], the EVMS-TPI formalism is particularly interesting for dense polymers, where up to 85-95% of the space can be pre-excluded, thus leading to speed-up factors of 10-20 compared to random insertions.

3.1.2. The ratio between concentrations and solubilities at equilibrium

In bulk models with 3D periodic boundary conditions, the number of gas molecules in the polymer n_{pol} and the pressure are independent variables. However, in reality, n_{pol} depends on the external pressure p of the gas reservoir in contact with the polymer matrix and on the temperature T. If an external gas is in equilibrium with the gas molecules inserted into the matrix, the chemical potential for the gas in the gas phase, μ_{gas}, has to be equal to the chemical potential for the gas in the polymer phase, μ_{pol} [30, 33]. For rigid molecules, the equality of the chemical potentials in both phases implies that the difference between the gas excess chemical potentials in the two phases is related to the ratio of their concentrations $C = n/V$ [84]:

$$\Delta\mu^{ex} = \mu_{pol}^{ex} - \mu_{gas}^{ex} = k_B T \ln \frac{C_{gas}}{C_{pol}} \tag{5}$$

with C_{gas} being the concentration of the gas in the gas phase and C_{pol} being the concentration of the gas in the polymer phase. Eqs. (4-5) lead to a simple relationship between the ratio of the concentrations and the ratio of the solubilities in both phases:

$$\frac{C_{gas}}{C_{pol}} = \exp\left(\frac{\Delta\mu^{ex}}{k_B T}\right) = \frac{\exp\left(\frac{-\mu_{gas}^{ex}}{k_B T}\right)}{\exp\left(\frac{-\mu_{pol}^{ex}}{k_B T}\right)} = \frac{S_{gas}}{S_{pol}} \quad \text{or alternatively} \quad \frac{C_{pol}}{C_{gas}} = \frac{S_{pol}}{S_{gas}} \tag{6}$$

3.1.3. Pure gas simulations

Prior to inserting the gas molecules into the polymer matrix, the gases have to be simulated in their pure phase at the temperature of interest, *i.e.* 308 K. N_2 [85], CH_4 [86] and CO_2 [87] were represented by all-atom models. For nitrogen, the centre-of-mass carried a charge twice as large and opposite in sign to that on the N atoms because of its quadrupole nature. All molecules were kept rigid using constraints [71, 72] to ensure a correct equipartition of the kinetic energy [88]. A series of separate MD simulations were carried out for 10000 ps under *NVT* conditions on systems of 1000 N_2, 512 CH_4 and 512 CO_2 molecules, respectively, using box sizes initially determined from the ideal gas law in the 0-100 bar range. Following equilibration, their average pressures p (corresponding to the imposed fixed volumes) were extracted directly from the results of the MD simulations. Solubilities were obtained from standard TPI analyses (Section 3.1.1) of the configurations stored at intervals of 10 ps over the last 9000 ps. The data was fitted to analytical functions in order for the concentrations in the gas phase $C_{gas}(p)$ and the corresponding solubilities in the gas phase $S_{gas}(p)$ to be known at any pressure up to 100 bar. The analytical functions and the fits are provided in the Supp. Info. (Fig. S2 and Table S1).

3.1.4. The GCMC method associated to the EVMS formalism

The Grand Canonical Monte Carlo (GCMC) approach is well documented and includes several variants [44, 89]. Simulations are carried out at constant chemical potential, volume and temperature, which are referred to as μVT conditions. Gas molecules are exchanged between the polymer phase and a gas reservoir of constant composition and density acting as a buffer. Monte

Carlo moves are used to establish an equilibrium between the gas molecules in the static pre-stored polymer configurations and the gas reservoir. It should be noted that a gas reservoir does not have to be explicitly simulated during a GCMC simulation [44]. Indeed, $C_{gas}(p)$ and $S_{gas}(p)$ are already parametrized from the *NVT* simulations carried out on the pure gas phases (Section 3.1.3).

In spite of being commonly used [23, 26], GCMC can be quite inefficient when applied to dense materials, since random insertions of gas molecules within the matrix generally lead to low acceptance rates. As such, we have improved its efficiency by including the excluded-volume map sampling formalism (EVMS) [47-49], which screens out polymer regions of very low insertion probabilities. To our knowledge, the combination of GCMC with EVMS has not been reported yet. For a target pressure p, the procedure is as follows:

a) The polymer phase is first scanned to screen out that part of the volume where the insertion probability is quasi-zero due to interactions with atoms in the polymer. This gives rise to two parts for the polymer volume V_{pol}, the V_{in} part (where insertions will be attempted) and the V_{out} part (where they will not). The EVMS unbiaising factor u_b is defined as the fraction of the volume where insertions will be attempted:

$$u_b = \frac{V_{in}}{V_{in} + V_{out}} = \frac{V_{in}}{V_{pol}} \tag{7}$$

b) GCMC sampling then selects a gas molecule from a specific phase with a probability proportional to its concentration in that phase. The probabilities of choosing a gas molecule in the gas phase, p_{cg}, or a gas molecule in the polymer phase, p_{cp}, are thus $p_{cg} = \frac{C_{gas}(p)}{C_{gas}(p) + C_{pol}(p)}$ and $p_{cp} = \frac{C_{pol}(p)}{C_{gas}(p) + C_{pol}(p)}$, respectively.

c) Once a gas molecule has been chosen (either from the gas or from the polymer phase), the probability of that molecule being moved into the other phase is related to its Boltzmann factor for the energy change upon insertion, $\exp\left(\frac{-\Delta\Phi}{k_B T}\right)$. Trial moves include the transfer from the gas phase to the polymer phase, *i.e.* "insertions into the polymer" and back, *i.e.* "deletions from the polymer". For the gas phase, the aforementioned Boltzmann factor corresponds to the pre-determined $S_{gas}(p)$

(Eq. (4) and Section 3.1.3), whereas it has to be explicitly calculated for the polymer phase. Within the EVMS formalism, the probability of insertion into the polymer phase p_{ip} can then be written as:

$$\begin{aligned} p_{ip} &= \frac{\exp\left(-\frac{\Delta\Phi}{kT}\right)}{S_{gas}(p)+\exp\left(-\frac{\Delta\Phi}{kT}\right)} \\ &= \frac{u_b \exp\left(-\frac{\Delta\Phi}{kT}\right)_{in} + (1-u_b)\exp\left(-\frac{\Delta\Phi}{kT}\right)_{out}}{S_{gas}(p)+u_b \exp\left(-\frac{\Delta\Phi}{kT}\right)_{in} + (1-u_b)\exp\left(-\frac{\Delta\Phi}{kT}\right)_{out}} \approx \frac{u_b \exp\left(-\frac{\Delta\Phi}{kT}\right)_{in}}{S_{gas}(p)+u_b \exp\left(-\frac{\Delta\Phi}{kT}\right)_{in}} \end{aligned} \tag{8}$$

the right-hand approximation being due to the fact that insertions into the screened-out part of the polymer phase are essentially associated to Boltzmann factors of zero. Similarly, the probability of insertion into the gas phase p_{ig} has to take into account the bias of the EVMS method:

$$p_{ig} = \frac{S_{gas}(p)}{S_{gas}(p)+\exp\left(-\frac{\Delta\Phi}{kT}\right)} \approx \frac{S_{gas}(p)}{S_{gas}(p)+u_b \exp\left(-\frac{\Delta\Phi}{kT}\right)_{in}} \tag{9}$$

The move is then accepted or refused depending on p_{ig} and p_{ip}. This process is repeated several million times until equilibrium is reached, *i.e.* the flux of molecules from the gas phase to the polymer phase is the same as that from the polymer phase to the gas phase. Detailed balance implies that:

$$p_{cg}p_{ip} = p_{cp}p_{ig} \;\Rightarrow\; \frac{C_{gas}(p)}{C_{gas}(p)+C_{pol}(p)}p_{ip} = \frac{C_{pol}(p)}{C_{gas}(p)+C_{pol}(p)}p_{ig} \tag{10}$$

Removing the common denominator and replacing p_{ip} and p_{ig} by their values (Eqs 8-9) leads to:

$$\begin{aligned} & C_{gas}(p)\frac{u_b \exp\left(-\frac{\Delta\Phi}{kT}\right)_{in}}{S_{gas}(p)+u_b \exp\left(-\frac{\Delta\Phi}{kT}\right)_{in}} = C_{pol}(p)\frac{S_{gas}(p)}{S_{gas}(p)+u_b \exp\left(-\frac{\Delta\Phi}{kT}\right)_{in}} \\ & \Rightarrow\; C_{gas}(p)u_b \exp\left(-\frac{\Delta\Phi}{kT}\right)_{in} = C_{pol}(p)S_{gas}(p) \end{aligned} \tag{11}$$

When averaged over many trial insertions into the polymer, Eq. (11) translates into the equality of the concentration and solubility ratios given in Eq. (6).

As mentioned above, the Monte Carlo moves are repeated many million times for each static polymer configuration, and convergence is deemed to be attained once the number of gas molecules in the polymer phase stabilizes. Averaging over a large range of stored configurations is particularly important in the case of the soluble gases as their solubility can markedly differ from one configuration to another (even in the absence of volume swelling). In the present case, the typical numbers of moves amounted to 50 million for CH_4 and N_2 and 200 million for the very soluble CO_2. They were carried out on at least 50 stored configurations of the pure polymer and analysed simultaneously on multiprocessor servers. As for the iterative EVMS-TPI approach [33, 34], the EVMS formalism is very efficient when combined with GCMC as it leads to speed-up factors of 10-20 compared to random insertions. However, the main disadvantage of the GCMC approach remains that it does not take into account the effects of loading on the polymer, *i.e.* the possible dilation and relaxation of the matrix.

3.1.5. The iterative pressure TPI-MD method for single-gas sorption

An alternative approach that does take into account the changes during sorption is the iterative *p*-TPI-MD technique designed by Van der Vegt et al. [30, 33]. Eq. (6) implies that if the applied pressure on a polymer+gas simulation box, $p_{applied}$, corresponds to that of an external gas in equilibrium with the actual gas load, $C_{pol}(p)/ C_{gas}(p)$ should intersect with $S_{pol}(p)/ S_{gas}(p)$ at that specific $p_{applied}$. As for GCMC, $C_{gas}(p)$ and $S_{gas}(p)$ can be obtained from the pure gas simulations. For the polymer phase, an initial guess for the number of gas molecules to load into the polymer n_{toload} can be made based on the infinite dilution solubility $S_{pol}(0)$ coupled with $C_{gas}(p)$ and $S_{gas}(p)$ over a small pressure interval (*e.g.* 0-2 bar). The n_{toload} used here were 20 for N_2, 50 for CH_4 and 100 for CO_2. All of them corresponded to less than 0.5 bar at low pressures, but were expected to lead to much larger changes in the pressure at higher concentrations in the polymer.

The required number of penetrant molecules, n_{toload}, is then inserted into the polymer using an adaptation of the EVMS-TPI method [35]. The system is first simulated under *NVT* conditions for ~100 ps to thermally equilibrate, before being switched to ***NPT*** conditions for 2000 ps in order for the system to relax. At low loadings, the initial pressure applied on the polymer+penetrant box,

$p_{applied} = p_1$, is set to 1 bar. The first 1000 ps are generally sufficient for the box size and shape to adjust to the increased load, and the last 1000 ps can then be used for post-analyses. From the average concentration of the gas in the polymer phase $\left\langle C_{pol}(p_1) \right\rangle = n_{pol} / \left\langle V \right\rangle$ and the average solubility of the gas in the polymer phase $\left\langle S_{pol}(p_1) \right\rangle$ at that initial guess pressure p_1, the quantities $\left\langle C_{pol}(p_1) \right\rangle / C_{gas}(p)$ and $\left\langle S_{pol}(p_1) \right\rangle / S_{gas}(p)$ are plotted separately as a function of the variable pressure p of the gas phase. The point of intersection of the two curves, $p_{intersect}$, provides the second approximation for the required pressure, $p_{applied} = p_2$. Another simulation of the gas in the polymer phase is conducted at p_2, which can then be used to obtain a third estimate and so on. These subsequent iterations are carried out over production periods of 1000 ps until convergence is attained, *i.e.* $p_{applied} = (p_{intersect} \pm 1$ bar). The typical number of iterations to achieve convergence is usually of the order of 3-4 for N_2 or CH_4, but it can increase up to 30 for CO_2. Once $p_{applied}$ has been iterated up to convergence for a total number of n_{pol} gas molecules in the polymer, a new set of n_{toload} molecules is then inserted into the polymer and the procedure is repeated to get the iterated pressure corresponding to the new n_{pol}. This continues up to ~60-70 bar [30, 33].

This technique allows for the prediction of the whole sorption curve whilst correctly taking into account the associated relaxation behaviour. However, it can become computationally expensive if many iterations are required to obtain convergence due to a combination of dilation and slow relaxation mechanisms in the loaded polymer systems. In addition, fixed steps in the increased numbers of molecules lead to smaller changes in pressures at low loadings so the spacing between the points is not always regular in pressure.

3.1.6. The iterative GCMC-MD method for single-gas sorption

As noted in the Introduction, both the advantages of Monte Carlo (Section 3.1.4) and molecular dynamics (Section 3.1.5) can be combined by alternating cycles of GCMC sampling with *NPT* MD simulations [29, 39-42]. GCMC is used to adjust the numbers of penetrants within the polymer matrix, while MD allows for the system to relax back to the required pressure following the change in the number of penetrants. Several GCMC-MD cycles are generally required before Eq. 6 is satisfied, hence its iterative character.

The initial estimate of the number of penetrants to insert at a target pressure of 1 bar is obtained from a first GCMC simulation on a set of up to 50 pure polymer configurations. Once converged, an optimum configuration in terms of the number of gas molecules is selected from the GCMC sampling. The required number of penetrants is known from the average of the converged runs over the 50 configurations. If the optimum configuration has a few excess molecules, these are deleted randomly. If it has a few missing molecules, which is rare, they are added using the loading adpatation of the EVMS-TPI method. The chosen configuration is then simulated for 100 ps of *NVT* MD in order to establish thermal equilibrium, before being switched to ***NPT*** conditions for a further 1900 ps. This allows for the box to adjust to the loading. A second phase of GCMC sampling is then carried out, still at 1 bar, over a range of stored configurations from the end of the first ***NPT*** MD simulation. As before, a new optimum configuration is selected from the final GCMC configurations. Following *NVT* MD, 900 ps of ***NPT*** MD are usually sufficient for the system to relax since the number of penetrants added is much less than at the first iteration. The iterative process then continues with alternating GCMC and MD phases until convergence in the number of sorbed penetrants occurs, *i.e.* the concentration and solubility ratios coincide (Eq. 6). As several GCMC-MD cycles are required to obtain convergence, the typical numbers of moves in a single GCMC phase can be reduced to 5 million for CH_4 and N_2 and to 20 million for CO_2. Subsequent iterative GCMC-MD simulations are then performed in the same way at different pressures, *i.e.* at 2, 5, 10, 20, 40 and 60 bar in the present study.

As for the iterative *p*-TPI-MD approach, the whole sorption curve can be predicted while allowing for the polymer to relax properly. The number of iterative cycles is again typically ~5 for N_2 and CH_4 but can also become quite large for plasticizing penetrants, *i.e.* ~30-40 for CO_2 due to the volume dilation which leads to slow convergence.

3.2. Single-gas sorption in the model 6FDA-6FpDA polymer matrix

CH_4, N_2 and CO_2 sorption isotherms were all obtained separately in the ~50000-atom bulk 6FDA-6FpDA matrix over the 0-60 bar interval using either the GCMC (Section 3.1.4), the iterative *p*-TPI-MD (Section 3.1.5) or the iterative GCMC-MD (Section 3.1.6) approaches. The total number

of gas molecules in the polymer at pressure p, $n_{pol}(p)$, was converted into the gas concentration $C_{pol}(p)$ in cm^3(STP)/(cm^3 polymer) by:

$$C_{pol}(p) = \frac{n_{pol}(p)}{V_{pol}(p)} \cdot \frac{k_B\, T^{STP}}{p^{STP}} \tag{12}$$

with T^{STP} and p^{STP} being the standard temperature and pressure (STP: 273.15 K; 1.013×10^5 Pa). Concentrations expressed in cm^3(STP)/(cm^3 polymer) are usually referred to as cm^3(STP)/cm^3.

The GCMC, iterative p-TPI-MD and iterative GCMC-MD model single-gas $C_{pol}(p)$ in the 6FDA-6FpDA matrix are compared for N_2 in Fig. 2a, CH_4 in Fig. 2b and CO_2 in Fig. 2c (symbols). The standard errors were calculated using a blocking method from the root mean square deviations in the data and the estimated statistical inefficiency, which stems from the degree of correlation in the data [89]. For the iterative p-TPI-MD, the errors are principally on the pressures, hence on the x-axis; there are small errors on the concentrations due to volume fluctuations but these are not distinguishable on the scale of the plot. For the GCMC and the iterative GCMC-MD, the errors are on the concentrations, hence on the y-axis. Due to the sufficient amount of sampling, the errors were systematically found to be smaller than the sizes of the symbols in Fig. 2. A representation with the symbols being "made transparent" in order to better see the error bars is provided in the Supp. Info. (Fig. S5). Consequently, the errors on the other analyses, which are directly linked to the uptake curves, were also very small.

As expected from glassy polymers, the $C_{pol}(p)$ for small gases are concave to the pressure axis, *i.e.* they have the shape of a Type I adsorption isotherm [90]. These are usually fitted over the whole pressure range to the single-gas equation of the dual-mode sorption (DMS) theory [91]:

$$C_{pol}(p) = k_D\, p + C'_H \frac{b\, p}{(1 + b\, p)} \tag{13}$$

where k_D is the Henry's law solubility coefficient, C'_H is the Langmuir sorption capacity and b is the Langmuir affinity parameter. The $C_{pol}(p)$ model gas concentrations do fit very well to the form of Eq. (13), and their respective DMS-fits are the lines displayed in Fig. 2. Also shown for comparison are the DMS-fits extracted from the single-gas experimental data of Coleman et al. [53], which were measured over the 0-60 bar pressure range. The DMS parameters used in Fig. 2 are provided in Table S4 (Supp. Info.). Another point to consider is the effect of system size. As explained in the

Introduction, our choice of a large 15-chain ~50000 atom 6FDA-6FpDA matrix stems from a former study of CO_2 sorption on three 3-chain systems (~10000 atoms) of the same polymer [33]. Fig. 2d compares the CO_2 sorption curves calculated with the *p*-TPI-MD method for each of the initial 3-chain matrices [33] with that obtained for the 15-chain matrix used in this work.

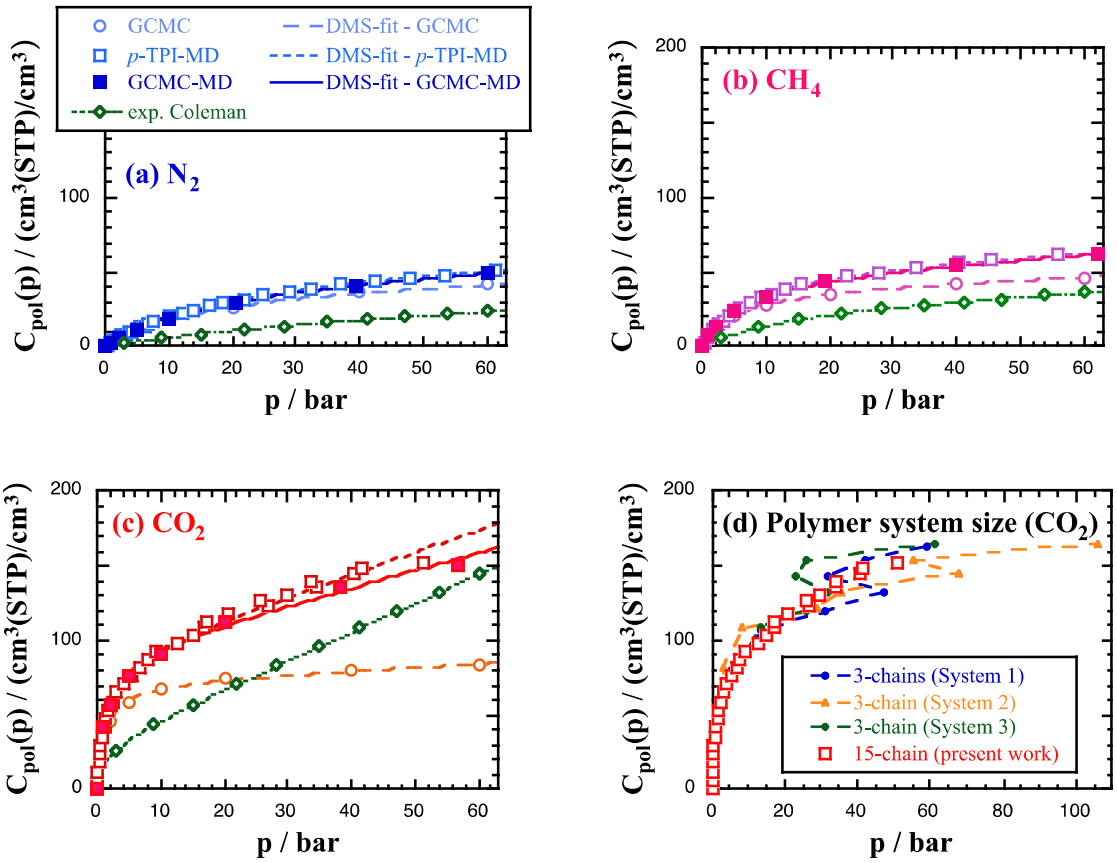

Fig. 2. Single-gas concentrations $C_{pol}(p)$ (symbols) for **(a)** N_2, **(b)** CH_4 and **(c)** CO_2 in the 6FDA-6FpDA matrix as a function of the pressure *p* obtained using either the GCMC only, the iterative *p*-TPI-MD or the iterative GCMC-MD method. In all cases, the standard errors are less than the size of the symbols and the lines are fits to the single-gas DMS form of Eq. (13). The diamonds are single-gas DMS fits based on the experimental results of Coleman et al. [53]. **(d)** The *p*-TPI-MD results for CO_2 sorption in former 3-chain models of 6FDA-6FpDA [33] compared with those for the 15-chain model under study here (white squares in Fig 2c).

An alternative representation of Fig. 2 showing the three gases on the same graph for each method is provided in Fig. S7 (Supp. Info.). At any particular pressure *p*, gas concentrations in the glassy matrix vary in the order CO_2 > CH_4 > N_2, *i.e.* in the same order than their critical

temperatures [92]. Fig. 2d shows the clear diminution in statistical fluctuations when using larger matrices, although as noted before, averaging over several simulation boxes of the same size [20, 23, 28, 29, 33, 38] also improves the statistics. When quantitatively comparing model and experimental uptake curves (circles and squares vs diamonds in Fig. 2), converged solubilities are often found to be enhanced in the molecular models [28, 29, 33, 93]. These differences are almost unavoidable and originate from the limitations associated to both models and experiments. Indeed, even if the force-field parametrization is known to have a limited impact on model sorption in 6FDA-based polymers [33], such molecular models remain classical and inevitably simplified with respect to a real membrane. They also represent "freshly-made" and "pure" polymers, and as such, their entire void-space is accessible to penetrant molecules. This is not the case for experimental samples of similar densities, which depend on many factors other than their chemical structure (precursors, molecular weights, solvents, thermal treatments, membrane thickness, aging ...) [61, 62, 94-97]. As such, impurities, remaining solvent molecules, defects and long-time relaxations (which are not accessible to the MD timescale) [29, 98-100] usually lead to a more restrained available void-space. In spite of these drawbacks, molecular models are still able to predict experimental sorption curves within a factor of 1 to 2 and provide model systems on which theoretical predictions can be tested [89]. In addition, since the differences are usually of the same order of magnitude for the various gases, model sorption selectivities often end up being in good agreement with the experimental values (see later).

When comparing the simulation techniques (Fig. 2), the uptake curves obtained by the iterative *p*-TPI-MD and GCMC-MD approaches, which both allow for the local relaxation of the polymer, are almost identical. On the other hand, GCMC on its own predicts uptake curves that might seem slightly closer to experiment, at least when the plasticizing effect of the gas is limited (Fig. 2a-b). Not allowing for dilation artificially keeps the void-space restricted, and as such, closer to that expected from experiment. Unfortunately, GCMC becomes really problematic when the gas induces significant plasticization (Fig. 2c). Indeed, gases such as CO_2 or hydrocarbons are known to lead to substantial volume-swelling in glassy matrices [101-105]. This should be accounted for in the models [29], which is the case for both iterative approaches. However, GCMC on its own can be interesting for saving time, *e.g.* for multi-screening purposes [27, 28], providing that it is applied

to low-plasticizing penetrants or, when modelling a plasticizing penetrant, at relatively low uptakes only.

The uptake curves displayed in Fig. 2 can be presented either as a function of the pressure or as a function of the fugacity [8, 9, 14], but it does not change much their form (see Fig. S7d in the Supp. Info.). Fugacities have indeed the advantage of better representing the chemical potential [8-10, 13, 14, 20, 23, 26] even though, experimentally, they are less accessible than partial pressures. In the following part of this work, we will keep in the main text the pressure representation to be consistent with the 6FDA-6FpDA experimental data [53, 58]. Indeed, CO_2 in our ternary test mixture is only present at a small partial pressure, *i.e.* within a range where pressures and fugacities are quite similar (Fig. S7d).

Small volumetric changes in finite samples of polymers are complicated to detect experimentally and quite error-prone [98, 101, 104, 106], but model dilation is easier to obtain from the behaviour of the simulation box. Fig. 3a shows the comparative GCMC-MD volume swelling with respect to that of the pure polymer as a function of the pressure p for all three penetrants. Fig. 3b displays the volume swelling as a function of C_{pol}, and confirms that the actual volume change in both the iterative *p*-TPI-MD and GCMC-MD approaches is quasi-identical.

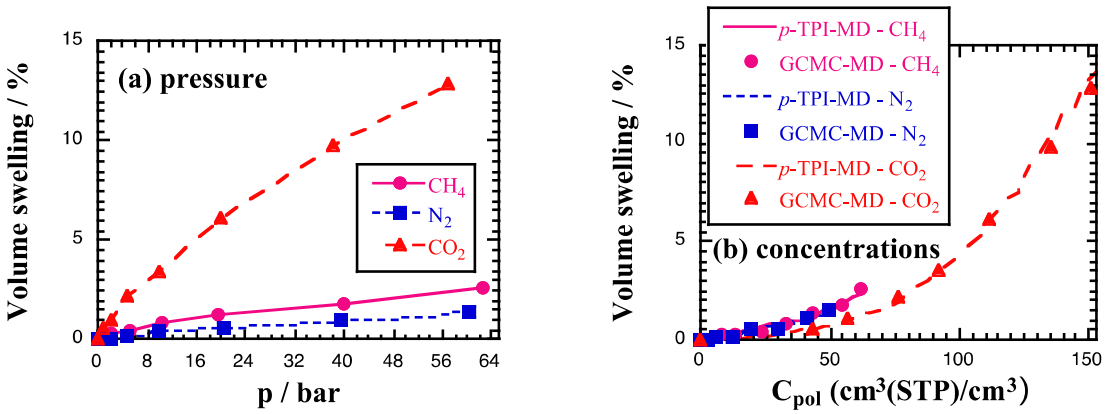

Fig. 3. Percentage of volume swelling upon single-gas uptake of CH_4, N_2 and CO_2 as a function of **(a)** the pressure in GCMC-MD simulations and **(b)** the gas concentration in the polymer obtained by both the iterative *p*-TPI-MD (lines) and the GCMC-MD (symbols) approaches

The volume swelling curves (Fig. 3) correlate well with the pressure and the penetrant concentrations in the polymer (Fig. 2). The behaviour of the density as a function of the loading is

also consistent with the volume swelling (see Fig. S8a, Supp. Info.). The dilation effect of CH_4 and N_2 in glassy polymers is usually less than 2-3% [34], and it reaches here ~2.6 % for CH_4 and ~1.4 % for N_2 at 60 bar. Based on these values, CH_4 can be classified as mildly-plasticizing and N_2 as non-plasticizing. On the other hand, the highly-plasticizing CO_2 leads to a much larger dilation [67], *i.e.* up to ~13 % at 60 bar. For each penetrant, the model partial molar volume (pmv) can be estimated from the limiting slope of the volume dilation vs. the number of sorbed molecules plot [107], *i.e.* it is obtained from linear fits on the last part of the curves in Fig. 3b. In our 6FDA-6FpDA matrix, the pmv for CO_2 is ~29 $cm^3\ mol^{-1}$, which agrees with the experimentally-reported pmv of 25-31 $cm^3\ mol^{-1}$ in polyimides [104, 108]. The pmv for CH_4 is ~15 $cm^3\ mol^{-1}$, which also compares well to experiment [98]. For N_2, the matrix swells a lot less and the model pmv is estimated to ~10 $cm^3\ mol^{-1}$.

At equivalent concentrations (*x*-axis of Fig. 3b), both CH_4 and N_2 appear to swell the polymer almost equally. These two penetrants are known to have similar kinetic diameters [109], *i.e.* ~3.8 Å for CH_4 vs ~3.6-3.7 Å for N_2. The larger swelling effect of CH_4 at equivalent pressures is thus related to its larger solubility. CO_2 has a smaller kinetic diameter (~3.3 Å), so, at the same concentration, it actually swells the polymer less than either CH_4 or N_2. Its very large volume swelling effect is thus due to its much higher solubility, which leads to subsequent plasticization of the polymer matrix. Experimentally, plasticization is usually considered as a drawback, since it leads to a decrease in the membrane permselectivity [10, 102].

Another issue with plasticizing gases is that it takes a much longer time for a CO_2+polymer system to relax in MD simulations with respect to non- or mildly-plasticizing gases. This is illustrated for the iterative *p*-TPI-MD approach by Figs. 4a-b, which compare the time relaxation of the density with that of $p_{applied}$ for two 6FDA-6FpDA simulation boxes containing either some strongly-plasticizing CO_2 (Fig. 4a) or some mildly-plasticizing CH_4 (Fig. 4b). The larger volume swelling upon CO_2 sorption leads to a gradually-decreasing density and as a consequence to a gradual rise in the solubility. This affects in turn $p_{applied}$, which significantly decreases with time. The iterated pressure is averaged over the stabilized period, *i.e.* the last 15000 ps in Figs. 4a-b. For such glassy matrices, the density relaxation is associated to very slow local dynamics, and it has been shown that the overall polymer mean-square displacements/librations over time-intervals of

1 ns are typically of the order of 1-2 Å^2 [6, 67, 110, 111]. In the iterative GCMC-MD approach, the slow CO_2-induced relaxation can be seen in the large number of iterations required to reach the equivalence of the concentration and the solubility ratios (Fig. 4c). The number of iterations is significantly higher than for CH_4 or N_2, which usually require less than 5 iterations to reach convergence. Indeed, for CO_2, the increase in the number of penetrant molecules at each GCMC step is largely offset by the volume swelling that occurs in the subsequent MD step. The increase in C_{pol} is thus relatively slow and S_{pol} does not decrease as much as expected. As shown in Fig. 4c, the convergence is quite difficult to assess, and it is deemed to be attained when the number of penetrants in the polymer remains constant. The average number of penetrants, volume and solubilities are here averaged over the last 5 iterations. In the literature, it has been reported that less than ~10 GCMC cycles are sufficient for CO_2 convergence to occur in smaller models of polyimides relaxed with ***NPT*** MD steps of either ~200 ps [39, 40] or ~1000 ps [42]. Other authors use 30 GCMC cycles and MD steps of ~2000 ps for PIM [29], or 60 GCMC cycles and MD steps of ~100 ps for polyimides [41]. The subtle relaxation effects illustrated in Fig. 4a are difficult to distinguish from the inherent statistical fluctuations in such systems, unless sufficient averaging is done. In our pure 49530-atom polymer bulk, fluctuations in the density are of the order of ±2 kg m^{-3} and this is also evident in Fig. 4b. For strongly-plasticizing penetrants (Figs. 4a-c), it is thus important to take into account as much as possible this slow relaxation [35]. On the other hand, this is lot less of a concern for non- or mildly-plasticizing penetrants (Fig. 4b).

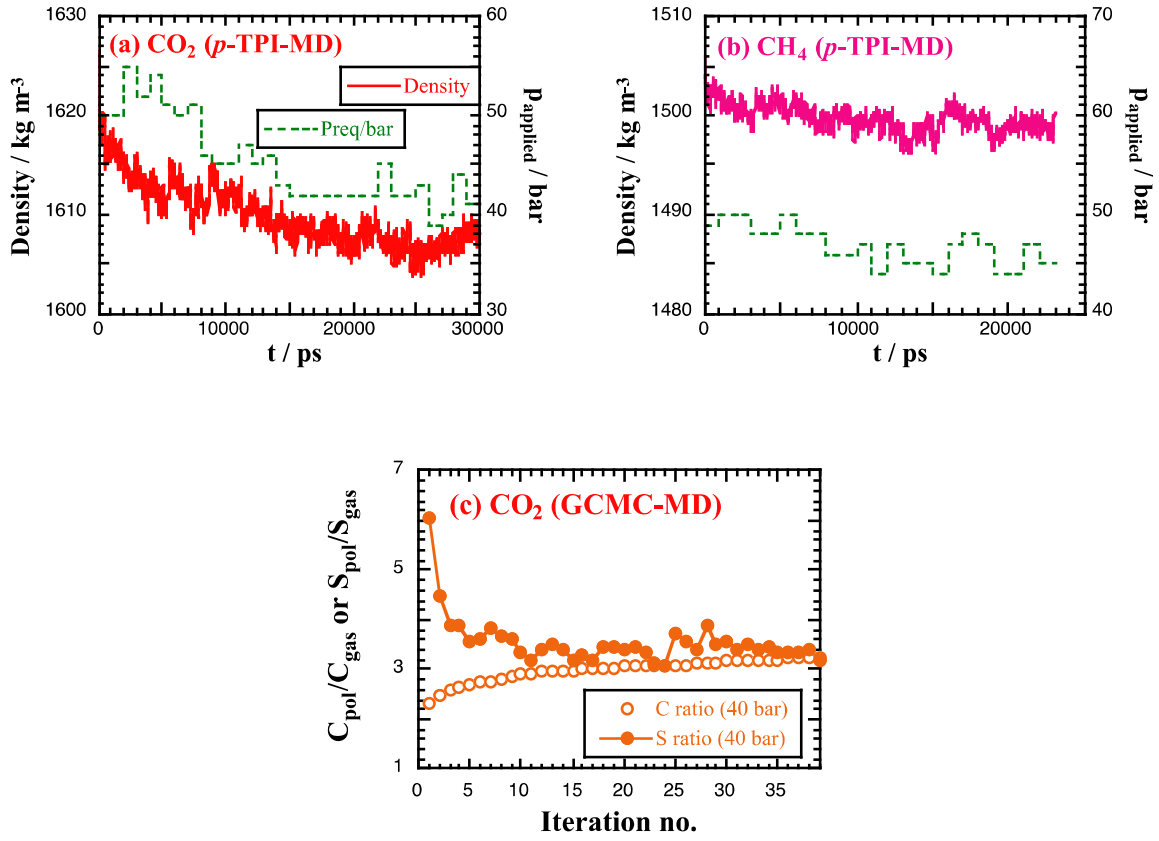

Fig. 4. Polymer relaxation phenomena associated with CO_2 uptake in 6FDA-6FpDA in both iterative approaches: the behaviour of the system density and the iterated pressure ($p_{applied}$) as a function of the simulation time in the *p*-TPI-MD approach for **(a)** CO_2 and **(b)** CH_4 at ~45 bar. **(c)** The concentration *C* and solubility *S* (polymer/gas) ratios (Eq. (6)) as a function of the number of iterations in the GCMC-MD approach for CO_2 at 40 bar.

Fig. 5 shows close-ups of the systems obtained from the *p*-TPI-MD simulations at a pressure of ~20 bar. The corresponding equilibrium boxes are displayed in Fig. S6 (Supp. Info.).

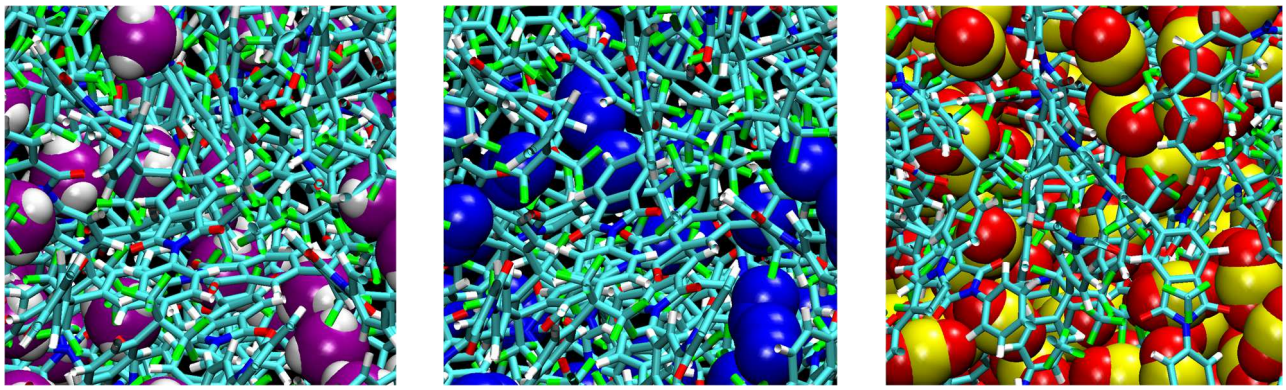

CH_4 **N_2** **CO_2**

Fig. 5. ~(20 Å)^2 close-ups of the 6FDA-6FpDA polyimide matrix loaded with ~20 bar of methane (C = pink, H = white), nitrogen (N = blue) or carbon dioxide (C = yellow, O = red).

Radial distribution functions can be used to characterize specific interactions sites for the gases in the membrane. As found before [6, 67, 110, 111], the closest interactions for the three gases are those with the protruding groups on the polymer, *i.e.* the 6FDA carbonyl oxygen and both types of fluorine groups. The gases thus access the available pre-existing void-space in the glassy matrix (Fig. 5). CO_2 plasticization leads to a general increase in the void space, which is basically affine to the amount of volume swelling [111]. This is confirmed by the mean-square end-to-end distance of the chains as a function of the relative linear change of the box dimensions, which is shown in Fig. S9 (Supp. Info.). Structural changes remain clearly very local in such glassy membranes. In addition, there are no signs of gas clustering.

In spite of their simplifications and their limited timescales, both iterative approaches are able to predict rather efficiently the ideal gas sorption selectivities in the polyimide under study. These are defined as:

$$\alpha^{S}_{A/B}(p) = \frac{S_A(p)}{S_B(p)} = \frac{C_{pol-gasA}(p)}{C_{pol-gasB}(p)} \tag{14}$$

and are displayed for all pairs in Fig. 6, along with the experimental selectivities of Coleman et al. [53] and Wang et al. [58]. The latter were obtained from fits to Eq. (13).

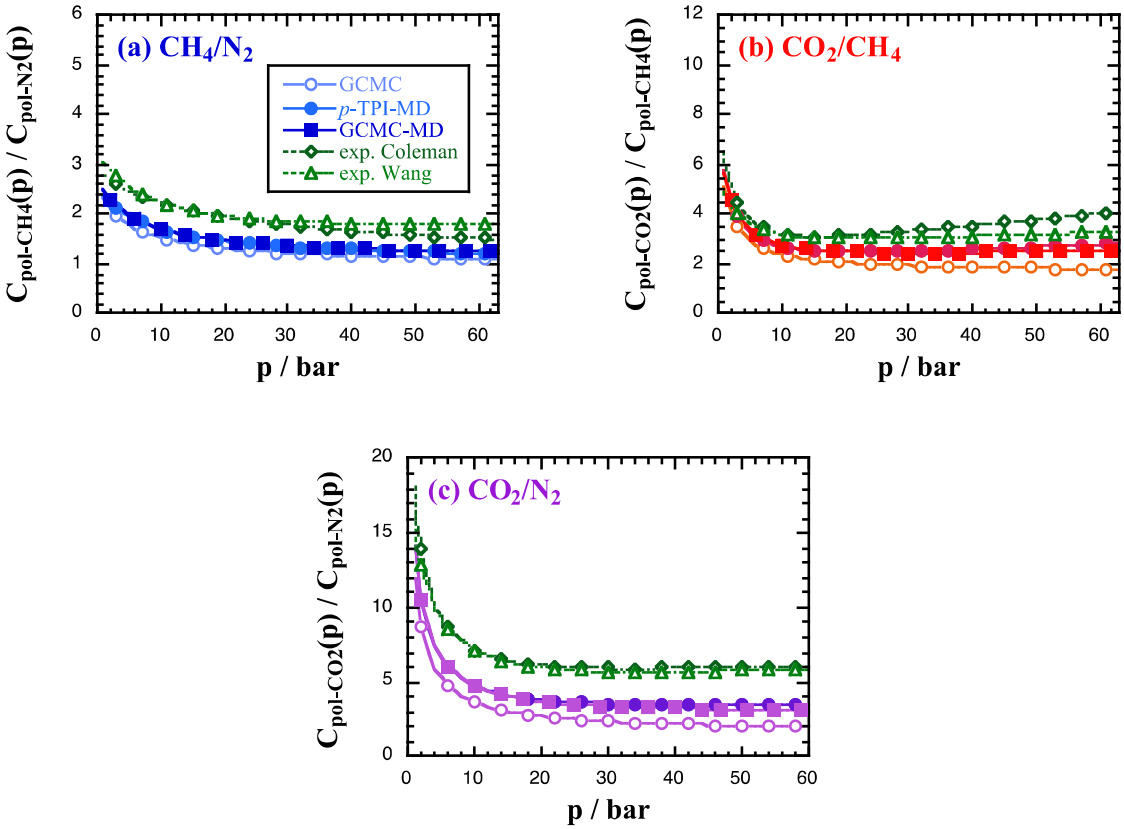

Fig. 6. Ideal sorption selectivities for **(a)** the CH_4/N_2, **(b)** the CO_2/CH_4 and **(c)** the CO_2/N_2 gas pairs in 6FDA-6FpDA as function of the pressure *p*. The circles and squares are from the models (GCMC = empty circles, *p*-TPI-MD = filled circles, GCMC-MD = filled squares) and the diamonds and triangles are the experimental data from Coleman et al. [53] and Wang et al. [58].

There are little differences between the selectivities predicted by the GCMC and the iterative approaches when CH_4 and N_2 are concerned (Fig. 6a). On the other hand, both the iterative model selectivities, which implicitly include dilation and polymer local relaxation effects, are again closer to the real systems when the strongly-plasticizing CO_2 is investigated (Figs. 6b-c). It should be noted that there is often a natural variability in experimental characterizations of the same polymer. Interestingly, in the range from 30 to 60 bar, the measurements of Coleman et al. for the CH_4/N_2 selectivity are closer to the iterative model values than to the measurements of Wang et al. (Fig. 6a). Similarly, the measurements of Wang et al. for the CO_2/CH_4 selectivity are closer to the iterative model values than to the measurements of Coleman et al. (Fig. 6b). The agreement between the iterative models and experiment is not as good for the CO_2/N_2 pair, since the N_2 model

uptake curve is enhanced by a factor closer to 2 than to 1 (Fig. 2a). However, in relative terms, the differences remain fairly small.

4. MIXED-GAS SORPTION IN POLYMERS

4.1. Methodology

All three techniques can be adapted to predict sorption curves in the case of exposure to mixed-gas reservoirs, *i.e.* under conditions closer to industrial gas separation applications [1, 112]. The general condition for equilibrium between the gas phase mixture of fixed composition and the polymer+penetrant system is once again that there is equality between their chemical potentials in the gas and polymer phases, but this now *applies to each penetrant*. For gas molecules modelled as rigid bodies, this means that equality of the concentration and solubility ratios, *i.e.* $C_{pol}/\ C_{gas} = S_{pol}/\ S_{gas}$ (Eq. (6)), must hold for each of the penetrants [113].

Two test cases were studied: the sorption of a binary 2:1 CH_4/N_2 and a ternary 16:8:1 $CH_4/N_2/CO_2$ mixture in contact with the 6FDA-6FpDA membrane under a large range of pressures, *i.e.* $0 \leq p_{mix} \leq 60$ bar. The total pressure p_{mix} is the sum of the partial pressures $p_{partial}$ of the gases in the respective mixtures. Both mixtures are consistent with the composition of natural gas [9, 65], although we note that previous simulation studies have mostly addressed the case of equimolar compositions [23, 26, 39]. This is an important point since the mixture composition can significantly affect the experimental solubility of the various penetrants [8, 9, 114]. In the present work, the intention is to compare "natural gas without plasticizer" and "natural gas with plasticizer".

4.1.1. The binary and ternary mixtures in the gas phase

A series of MD simulations were carried out for 10000 ps under *NVT* conditions at 308 K on eight 2:1 CH_4/N_2 and eight 16:8:1 $CH_4/N_2/CO_2$ systems in the gas phase. For the binary mixture, 512 CH_4 + 256 N_2 molecules were placed in boxes corresponding to the ideal gas volume at pressures of 1, 2, 5, 10, 20, 40, 60 and 80 bar. For the ternary mixture, 32 CO_2 molecules were added to the existing CH_4/N_2 systems. Following equilibration, their average pressures p_{mix} (corresponding to the imposed fixed volumes) were extracted directly from the results of the MD simulations. Solubilities $S_{gas}(p_{mix})$ were obtained from TPI analyses of the configurations stored at intervals of 10 ps over the last 9000 ps.

To parametrize the concentration of the pure mixtures over a 0-80 bar range for p_{mix}, the concentration-pressure data were fitted to the virial form of Eq. (15), which guarantees the ideal gas behaviour in the limit of low pressures:

$$C_{gas}(p_{mix}) = \frac{n_{mix}}{V_{gas}(p_{mix})} = \frac{10^{-22}}{k_B T}\left(p_{mix} + a\, p_{mix}^2 + b\, p_{mix}^3\right) \quad (15)$$

with n_{mix} being the total number of gas molecules, the factor of 10^{-22} accounting for the pressure being in bar (1 bar = 10^5 Pa) and the concentration being in molecules/nm^3. Similarly, the solubilities for each gas in the mixed-gas phase could be fitted quite satisfactorily to the quadratic form of Eq. (16):

$$S_{gas}(p_{mix}) = 1 + \alpha\, p_{mix} + \beta\, p_{mix}^2 \quad (16)$$

The mixed-gas phase data are displayed in the Supp. Info. (Figs. S3 and S4) along with the best-fit parameters obtained from non-linear least squares regression analyses (Tables S2 and S3).

Since the numbers of methane molecules in the gas phase are fixed, this allowed for interpolations of the methane concentration $C_{gas\text{-}CH4}(p_{mix}) = n_{gas\text{-}CH4}/V_{gas}(p_{mix})$ and solubility $S_{gas\text{-}CH4}(p_{mix})$ to be obtained at any pressure up to ~80 bar. The same analysis could be carried out for nitrogen and carbon dioxide, thus leading to their concentrations $C_{gas\text{-}N2}(p_{mix})$ and $C_{gas\text{-}CO2}(p_{mix})$ along with their solubilities $S_{gas\text{-}N2}(p_{mix})$ and $S_{gas\text{-}CO2}(p_{mix})$ over the whole range of p_{mix} in both mixed-gas phases.

4.1.2. The iterative number TPI-MD method for mixed-gas sorption

The iterative *p*-TPI-MD technique for single-gas sorption [30, 33] described in Section 3.1.5. cannot be used directly for mixed-gas feeds. Considering a mixed-gas reservoir of fixed composition in the gas phase, it is highly unlikely that a common pressure p_{mix} can be found to ensure that $C_{pol}(p_{mix})/ C_{gas}(p_{mix})$ coincides with $S_{pol}(p_{mix})/ S_{gas}(p_{mix})$ for every one of the components if the numbers of several types of gas molecules are fixed in the polymer phase. For this reason, the TPI-MD method was adapted to fix the applied pressure (rather than the number of penetrants) and then iterate to convergence the numbers of each type of penetrant present in the polymer phase. This adaptation is referred to here as the iterative *n*-TPI-MD. It has already been applied to the sorption of a binary CH_4/N_2 mixture in ~10000-atom models of 6FDA-mPDA and 6FDA-durene polyimides and the technical details have been given previously [34]. To summarize, the

adjustments in the numbers of sorbed molecules at each iteration are carried out based on the sign of the difference in C_{pol}/C_{gas} - S_{pol}/S_{gas} ratios, which indicate whether more penetrant molecules have to be added to (sign negative) or removed from (sign positive) the polymer phase. In the case of a binary mixture, the sum of $|C_{pol}/C_{gas} - S_{pol}/S_{gas}|$ for both penetrants has to be minimized in order to reach convergence. The difficulty is gauging the changes in the number of penetrants since the concentrations and solubilities of both species in the polymer phase are highly interdependent. It was thus rather complicated to automate for a binary mixture [34], and it is expected to be even more difficult for a general gas mixture. As such, the iterative *n*-TPI-MD approach was used here to study the sorption of the binary 2:1 CH_4/N_2 mixture (in order to compare it with the iterative GCMC-MD method), but it was not adapted to the ternary mixture. The typical number of iterations for this binary mixture were ~10-15 at the highest pressures. A significant advantage of the *n*-TPI-MD method is that the penetrant concentrations in the polymer phase can be obtained at preset and more regular pressure intervals than in the original iterative *p*-TPI-MD method (see *e.g.* Fig. 2c).

4.1.3. The iterative GCMC-MD method for mixed-gas sorption

Unlike the iterative *p*-TPI-MD approach, the iterative GCMC-MD method for single-gas sorption can be easily extended to the case of mixed-gas feeds. It also has the advantage of randomizing the positions of the penetrants at each iteration. The details are identical to those given in Section 3.1.6. The optimal final configuration at the end of the GCMC phase is selected and, if necessary, the numbers of penetrants are adjusted as described before. This configuration is then used as the start for the MD relaxation phase. Mixed-gas GCMC-MD simulations were performed for both the binary 2:1 CH_4/N_2 and the ternary 16:8:1 $CH_4/N_2/CO_2$ mixtures. For each case, the typical number of iterations was ~15 and the results were averaged over the last 5 iterations. With a limited partial pressure of CO_2 in the ternary mixture, there was no need to carry out as many iterations as in Fig. 4c. However, in general, this will depend on the composition of the mixture. As for the single-gases, the GCMC-only approach was also included in our study but, given its limitations for plasticizing penetrants, it was only applied to the binary mixture.

4.2. Mixed-gas sorption of a binary 2:1 CH_4/N_2 and a ternary 16:8:1 $CH_4/N_2/CO_2$ mixture in the model 6FDA-6FpDA matrix

The sorption of the binary CH_4/N_2 mixture was modelled in the ~50000-atom bulk 6FDA-6FpDA model matrix at pressures p_{mix} of 1, 2, 5, 10, 20, 40 and 60 bar using the GCMC, iterative *n*-TPI-MD and iterative GCMC-MD techniques as outlined in Section 4.1. The sorption of the ternary 16:8:1 $CH_4/N_2/CO_2$ mixture was modelled at the same pressures, but using only the iterative GCMC-MD approach. The equilibrium concentrations of all penetrants within the polymer are displayed as a function of the p_{mix} pressure in Fig. 7a for the binary and in Fig. 7b for the ternary mixtures. An alternative representation comparing the C_{pol} for each gas as a function of the gas fugacity in both mixtures is provided in the Supp. Info. (Fig. S10). For the GCMC-based and the *n*-TPI-MD methods, the errors are on the numbers and hence on the concentrations. As for the single-gas uptakes, they were smaller than the sizes of the symbols in Fig. 7 (see Fig. S5b, Supp. Info.). Fig. 7c compares the total gas uptake for both mixtures in the 6FDA-6FpDA matrix.

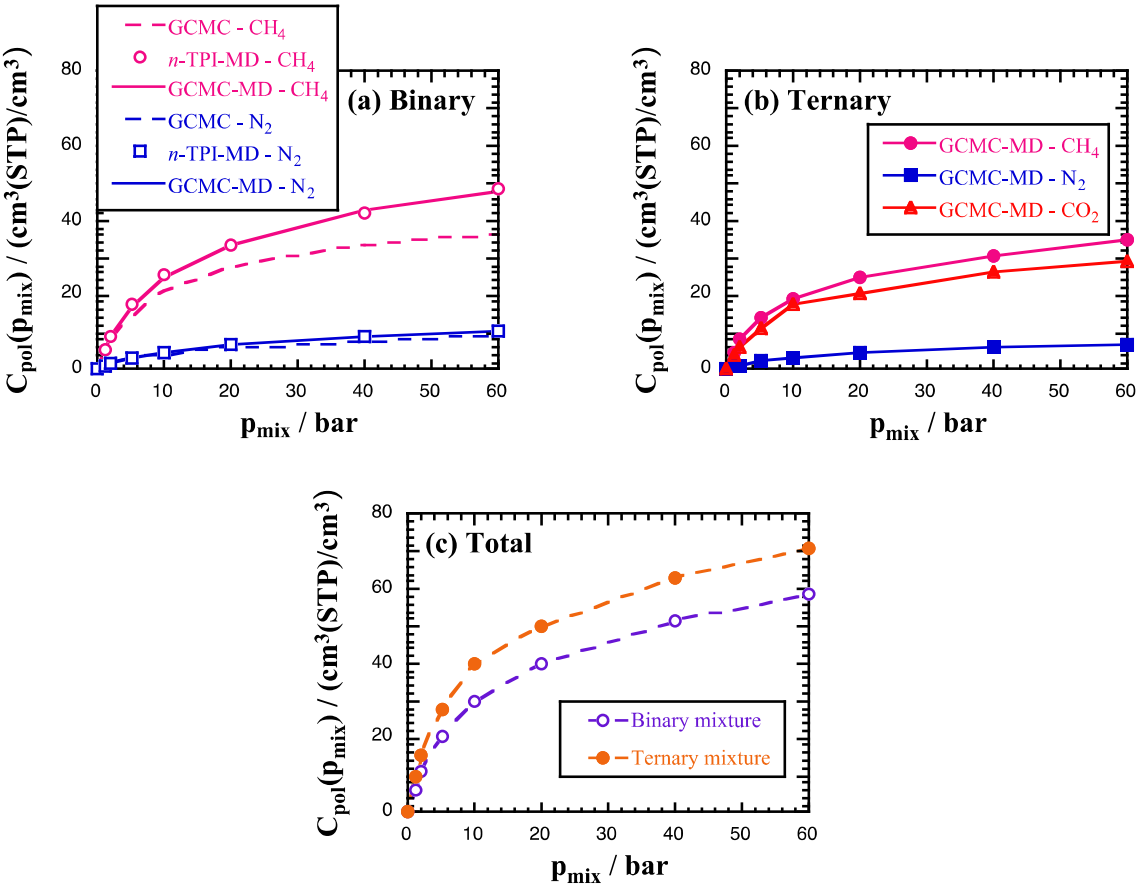

Fig. 7. $C_{pol}(p_{mix})$ for CH_4, N_2 and CO_2 in the 6FDA-6FpDA matrix as a function of the pressure p_{mix} that would have an external **(a)** binary 2:1 CH_4/N_2 or **(b)** ternary 16:8:1 $CH_4/N_2/CO_2$ gas reservoir. For the binary mixture, all three GCMC, *n*-TPI-MD and GCMC-MD techniques have been used. For the ternary mixture, only the GCMC-MD technique has been used. **(c)** is the GCMC-MD uptake of all the gases together for both binary and ternary mixtures. The standard errors are less than the size of the symbols.

It is clear from Fig. 7a that the iterative *n*-TPI-MD and GCMC-MD techniques provide identical results for the binary mixture within statistical errors. GCMC on its own underestimates the uptake of CH_4 (even in the absence of CO_2), and as shown by Anstine et al. [28], this is expected to get even worse in the presence of more plasticizing penetrants. It thus gives confidence that the iterative GCMC-MD can be used on its own for the ternary mixture (Fig. 7b). In the binary system, CH_4 and N_2 represent ~85% and ~15% of the sorbed molecules respectively, whereas their mixed gas phase proportions are 67% and 33%. In the ternary system, CH_4 and N_2 represent ~50% and ~10% of the sorbed molecules respectively, whereas their mixed gas phase proportions are 64% and 32%. On the other hand, CO_2, which was only present at 4% in the ternary gas mixture, now makes up ~40% of the sorbed molecules and increases the total gas uptake by more than 20%

(Fig. 7c). A highly-soluble penetrant can thus have a significant effect on competitive sorption, even if it is a contaminant at a very low partial pressure.

Koros et al. have extended the DMS theory for singles gases (Eq. (13)) to binary mixtures of gases A and B, based on the constants obtained from the DMS-fits of their respective single-gas uptake curves and their partial pressures p_A and p_B in the mixture [16, 17]. The mixed-gas concentrations in the polymer phase are then expressed as:

$$C_{pol-gasA}(p_{mix}) = k_{DA}\, p_A + \frac{C'_{HA}\, b_A\, p_A}{(1 + b_A\, p_A + b_B\, p_B)} \tag{17a}$$

$$C_{pol-gasB}(p_{mix}) = k_{DB}\, p_B + \frac{C'_{HB}\, b_B\, p_B}{(1 + b_A\, p_A + b_B\, p_B)} \tag{17b}$$

The predictions of the DMS theory for our binary mixture (Eqs. (17a-b)) based on the single-gas DMS-fits to the GCMC-MD results (Fig. 2c) are shown in Fig. 8a, along with the actual values from the mixed-gas simulations (symbols). A similar analysis was carried out for the ternary mixture by adding the CO_2 component to Eq. 21 and the results are displayed in Fig. 8b.

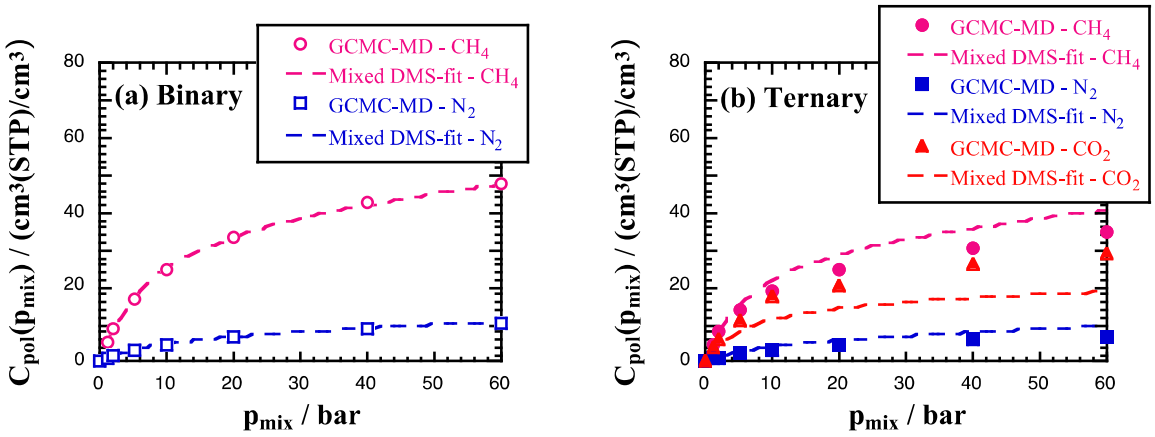

Fig. 8. Comparison between the sorbed gas concentrations in the 6FDA-6FpDA polymer matrix obtained directly from the mixed-gas GCMC-MD simulations (symbols) or by applying the mixed-gas DMS theory (Eq. 17, dashed lines) based on the parameters extracted from the fits to the single-gas uptake curves. **(a)** is for the binary and **(b)** is for the ternary system.

The DMS mixed-gas predictions are very close to the actual model concentrations for the binary CH_4/N_2 mixture (Fig. 8a). However, the agreement is a lot worse for the ternary mixture (Fig. 8b). Koros et al. have pointed out that the use of pure-gas sorption coefficients as applied to mixtures implies that the various gases behave independently except for the competition for the

unrelaxed volume fraction in the polymer. They also warn for possible deviations when the single-gas parameters can be altered by solubility or mobility-related effects [16, 17]. This is probably the case here for the highly-soluble CO_2, whose concentration is clearly underestimated by the mixed-gas DMS-fit, whereas both the CH_4 and N_2 concentrations are overestimated (Fig. 8b). Ricci et al. [14] and Gleason et al. [10] have indeed reported discrepancies between mixed-gas DMS-fits and experimental data for several glassy polymers. Both these authors showed that it is possible to improve the agreement by including multicomponent data in the parametrization, but it then lacks the predictive character of Eq. (17). Here, the DMS model has mainly been used for its simplicity as it is very straightforward to extract the parameters from the single-gas model uptake curves (Fig. 2a-c) and convert them to the mixtures via Eq. (17). There are nowadays far more accurate non-atomistic models in the literature and a comparative review has recently been published [22]. The NET-GP model is clearly to date the most powerful one to predict gas sorption [13, 115, 116]. However, it has a much higher level of complexity than the DMS model and, as such, it is beyond the scope of the present work.

Fig. 9 displays the percentage of volume swelling in the mixed-gas systems as a function of p_{mix} (Fig. 9a) and as a function of the total gas concentrations in the polymer (Fig. 9b-c). As for the single-gases, the behaviour of the density as a function of the mixed-gas loading is consistent with the amount of volume swelling (see Fig. S8b, Supp. Info.).

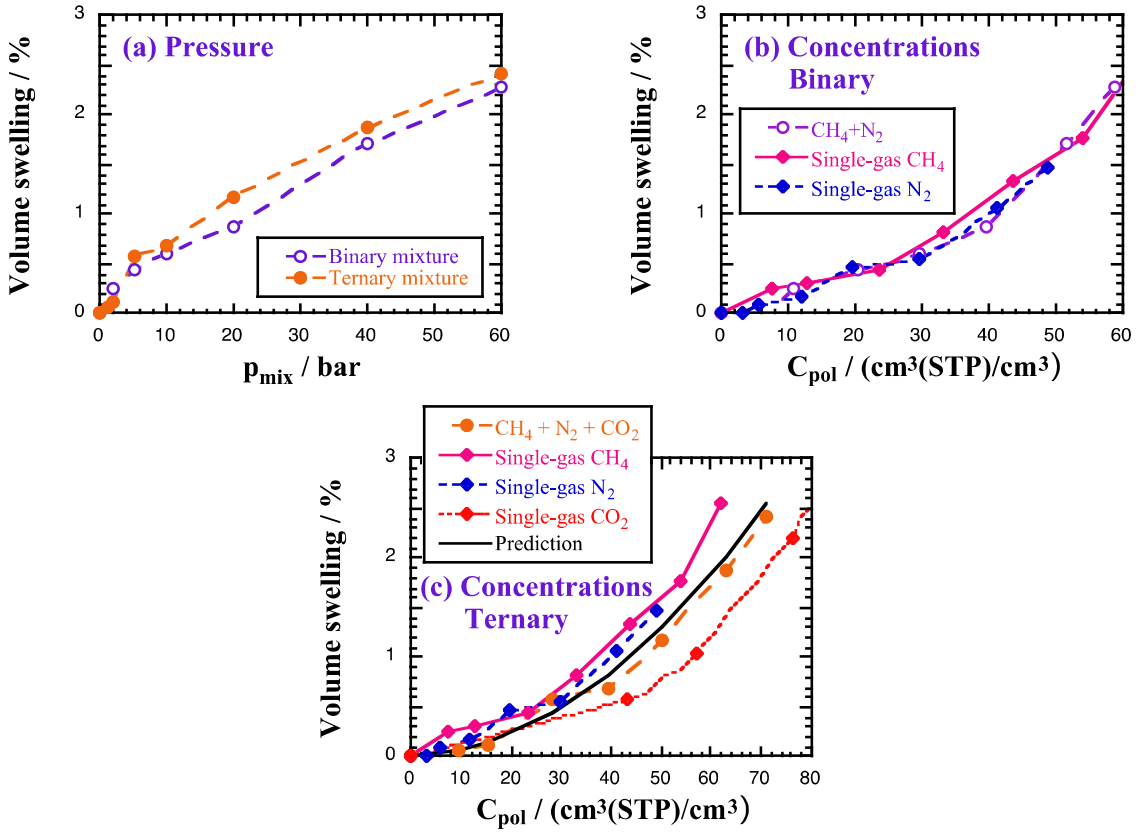

Fig. 9. Percentage of volume swelling as a function of **(a)** the pressure in the mixed-gas systems and **(b-c)** the total gas concentration in the polymer upon either mixed- or single-gas uptakes of CH_4, N_2 and CO_2. **(b)** is for the binary and **(c)** is for the ternary system. In **(c)** the black curve is a prediction based on the single-gas results (see text for details).

The volume swelling remains quite limited upon mixed-gas sorption of reservoirs containing mainly CH_4 and N_2. Indeed, it hardly reaches 2.5% at the highest p_{mix} in both mixed-gas systems (Fig. 9a). For our model of CO_2 in polyimides, plasticization has been shown to start above a concentration of ~40-80 $cm^3(STP)\ cm^{-3}$ [33, 67], in good agreement with experimental evidence [117, 118]. In our ternary system, the maximum CO_2 sorption is ~30 $cm^3(STP)\ cm^{-3}$ at 60 bar, which is below this threshold. However, there is clearly no need for plasticization to have an effect on selectivity [10]. If the volume swelling is plotted instead as a function of the total penetrant concentration within the matrix, the binary-mixture curve is quasi-superimposable with both the CH_4 and N_2 single-gas curves (Fig. 9b). As noted for the single-gas uptake curves (Fig 3), the amount of swelling induced by CH_4 and N_2 in the model polymer is close because of their similar kinetic diameters and it is larger on a *per* molecule basis than that of CO_2. For this reason, the

swelling in the ternary system is lower than in the binary system at equivalent total penetrant concentrations. A prediction of the volume change based on a penetrant mole fraction proportionality combination of the single-gas results is also shown in Fig. 9c (see Fig. S11 and Table S5 in the Supp. Info. for details). As expected, it matches reasonably well the actual data from the ternary system.

Fig. 10 shows close-ups of the binary and ternary mixture uptakes into the bulk 6FDA-6FpDA model matrix, once converged at pressures of 5, 20 and 60 bar. The corresponding equilibrium boxes are displayed in Fig. S6 (Supp. Info.).

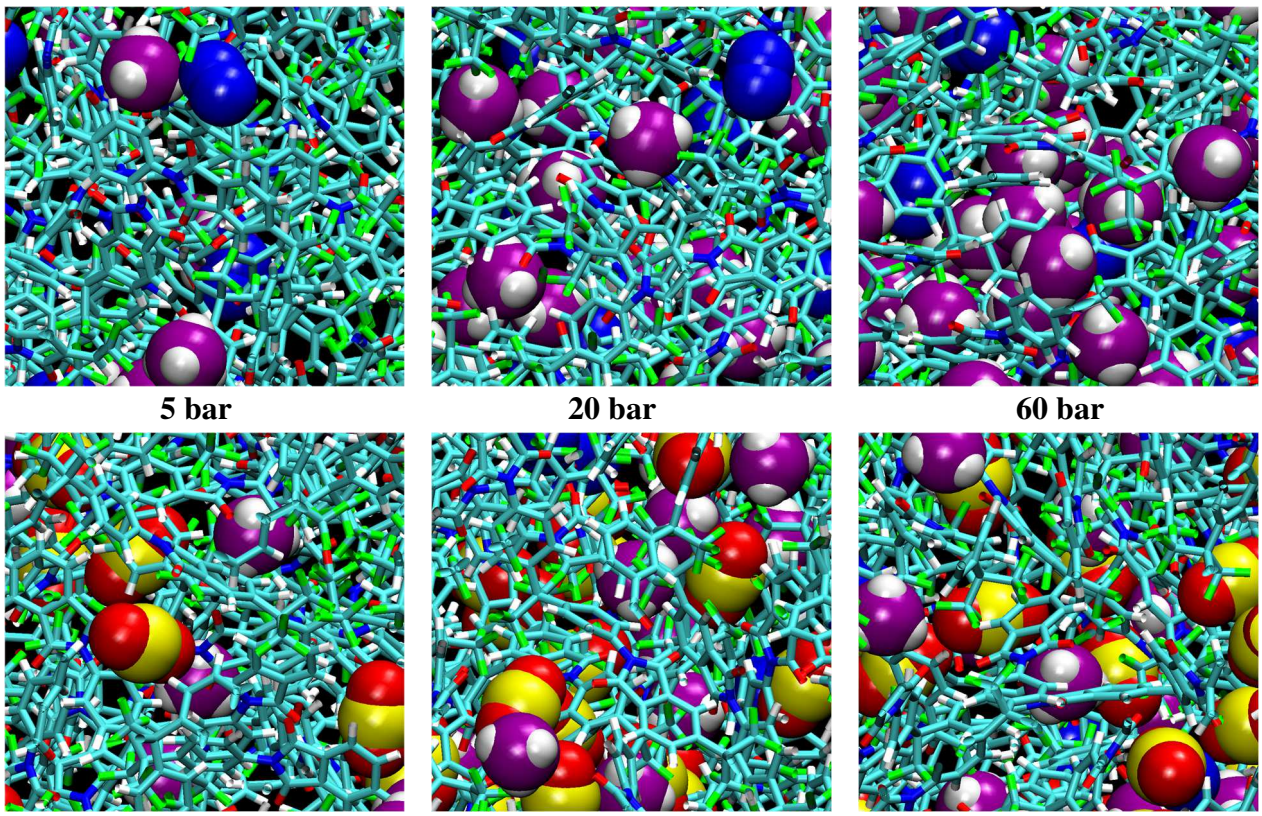

Fig. 10. ~(20 Å)^2 close-ups of the 6FDA-6FpDA polyimide matrix at three p_{mix} loadings of **(upper frames)** a binary 2:1 CH_4/N_2 and **(lower frames)** a ternary 16:8:1 $CH_4/N_2/CO_2$ mixture.

Fig. 11 compares the dimensionless solubility (Eq. (4)) of the various gases as a function of the total penetrant concentration C_{pol} under single- and mixed-gas conditions. These are found to superimpose for both binary (Fig. 11a) and ternary (Fig. 11b) systems. Furthermore, if each solubility curve is normalized by its infinite dilution limit, i.e. $C_{pol} = 0$, they all collapse onto a similar curve (Fig. 11c).

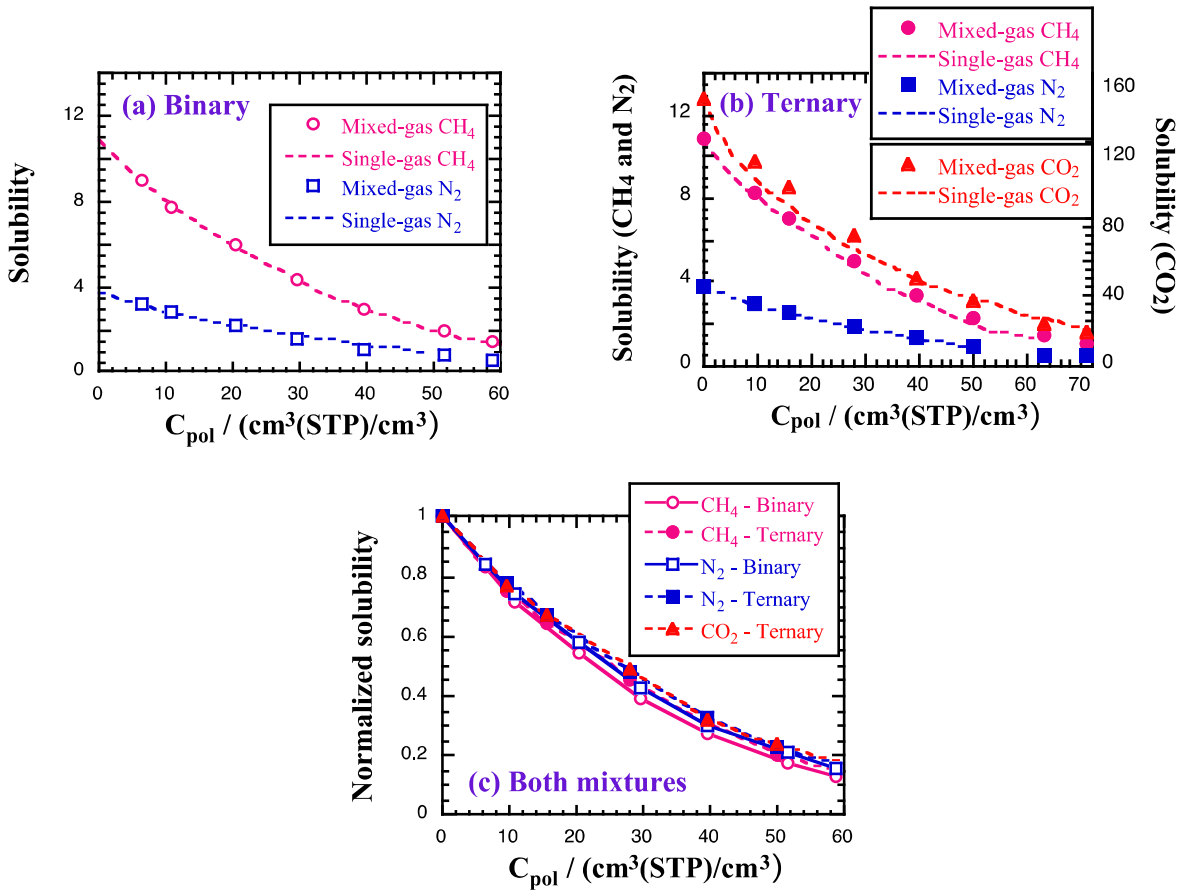

Fig. 11. CH_4, N_2 and CO_2 (dimensionless) solubilities (Eq. 4) as a function of the total gas concentration in the polymer for mixed- and single-gas uptakes in **(a)** the binary and **(b)** the ternary systems. In **(c)**, the dimensionless solubilities have been normalized by their value at $C_{pol} = 0$.

Fig. 11 shows that the gas molecules are apparently indifferent as to whether the systems are loaded with one gas or the other. This means that different penetrant molecules occlude about the same amount of volume to each other as they do to molecules of the same type. As such, the penetrants which are already present in the matrix simply reduce the volume available to a gas molecule and thus its possibilities of sorbing. It also suggests that the dominant interactions are between the penetrants and the polymer matrix. Vopička et al. [9] have reported similar correlations in experiments on CH_4 and CO_2 in PIM-1. They showed that the depression of CO_2 solubility produced by a given concentration of CH_4 in the polymer is very close to the depression of CH_4 solubility produced by the same molar concentration of CO_2 in the matrix. As such, they concluded that the ability of one penetrant to supress the solubility of the others is directly linked to its actual concentration sorbed in the matrix (and as such, to its own solubility), or in other words, that this

does not depend on the nature of the co-sorbent [9]. Genduso et al. [11] have reported a linear trend for mixed-gas CO_2 versus CH_4 solubilities in 6FDA-mPDA and related polymers, with the slope being the ratio between the solubilities at infinite dilution. This confirms the results displayed in Fig. 11c.

Fig. 12 compares the actual gas uptakes (left axes) under mixed- and single-gas conditions for the same partial pressure $p_{partial}$ of a specific gas. For the single gases, $p_{partial}$ is simply the total pressure. The right axes of Fig. 12 display the similarity factor for each gas as a function of its $p_{partial}$ as defined by Rizzuto et al. [23]:

$$\text{Similarity factor} = \left[1 - \frac{C_{pol}(\text{single-gas}) - C_{pol}(\text{mixed-gas})}{C_{pol}(\text{single-gas})}\right] \times 100 \qquad (18)$$

which characterizes the deviations in the mixture from the single-gas behaviour.

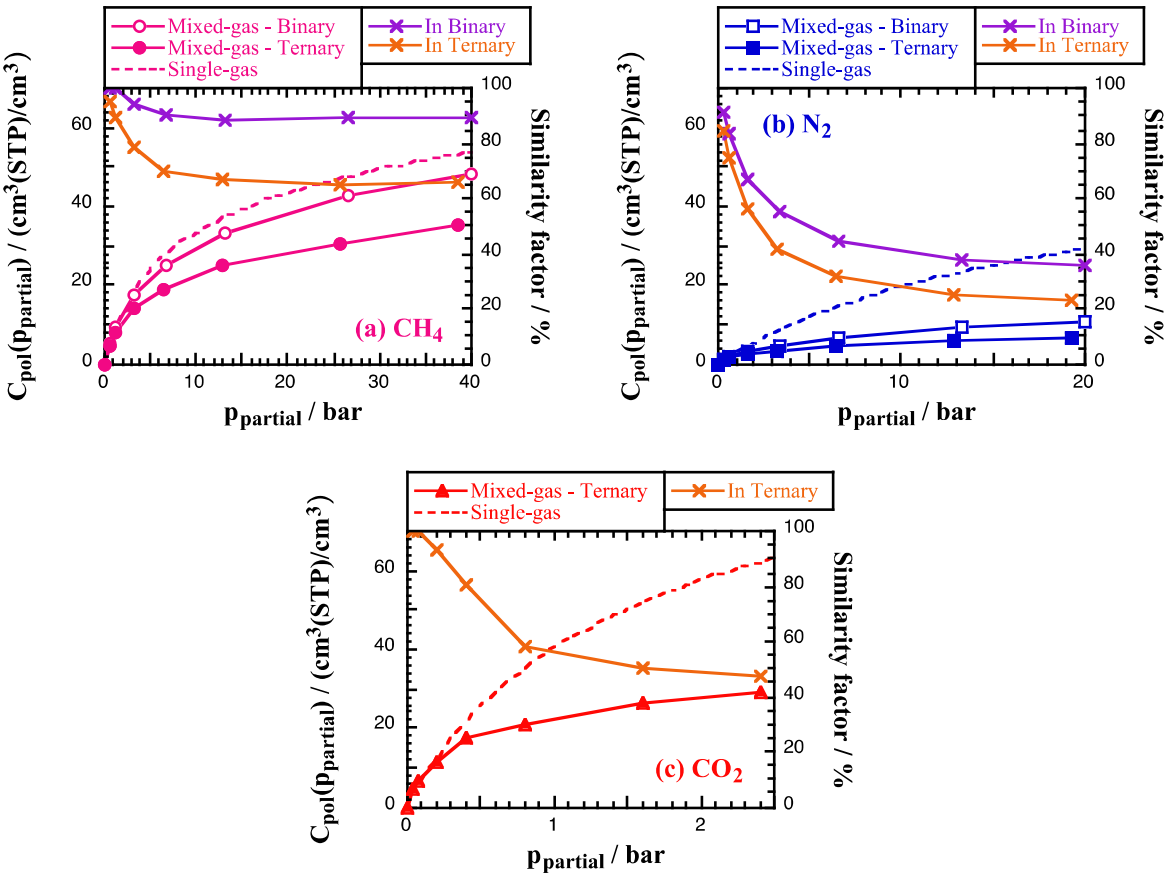

Fig. 12. Left axis: A comparison of $C_{pol}(p_{partial})$ for **(a)** CH_4 **(b)** N_2 and **(c)** CO_2 in the 6FDA-6FpDA polymer under binary 2:1 CH_4/N_2, ternary 16:8:1 $CH_4/N_2/CO_2$ and single-gas conditions as a function of the partial pressure $p_{partial}$ in a corresponding gas reservoir. Right axis: the similarity factors in % (Eq. (18)) for the binary and ternary mixtures.

Under mixed-gas conditions, competition occurs and the space occupied by one penetrant becomes unavailable to the other ones. The more condensable species tend to dominate and, as such, the sorption of the other penetrants is inhibited with respect to the single-gas uptakes. Indeed, in spite of their normalized solubilities in the polymer phase being similar (Fig. 11c), the actual effect of each penetrant at a specific p_{mix} is linked, via Eq. 6, to a combination of its affinity, *i.e.* its solubility in both the gas mixture and polymer phases, and its partial pressure, *i.e.* the composition of the mixture [8-10, 13, 16, 20]. This multi-factorial process makes mixed-gas conditions particularly difficult to characterize.

At equivalent $p_{partial}$ (Fig. 12), single- and mixed-gas uptake curves are not obtained under exactly the same conditions: the solubility in the mixed-gas phase is close but not necessarily the same as in the single-gas phase and the polymer volume swelling/relaxation effects are not identical

either. To better characterize the interference effects, it is useful to estimate the maximum uptake of each gas, while keeping the gas phase solubilities and concentrations, thus the chemical potential, equal to those in the gas mixtures and the polymer structures identical to those in the actual mixed-gas systems. As such, the GCMC method was rerun for each mixture on a set of 20 configurations taken from the last MD iteration with 5 million moves for both CH_4 and N_2 and 20 million moves for CO_2, but under two different conditions: i) with the solubilities of all the other penetrants in the polymer phase being artificially set to zero and ii) with all interactions re-switched on. Using a set of converged polymer+penetrant configurations pre-obtained via the iterative GCMC-MD method avoided the difficulties associated with using the GCMC method on its own (Fig. 2). Condition (i) gave an estimation of the maximum number of gas molecules n_{gas_max} that would have sorbed into the 6FDA-6FpDA matrix if it had been free from the interference of the other penetrants, while condition (ii) gave the actual number of sorbed gas molecules n_{gas} to ensure that the results were consistent with the converged values found before.

Comparisons between n_{gas_max} and n_{gas} are presented in Table 1 for both mixtures at p_{mix} of 40 and 60 bar. The ratio between n_{gas_max} and n_{gas} characterizes the efficiency of the sorption under mixed-gas conditions. The difference between n_{gas_max} and n_{gas} are those gas molecules excluded due to the competitive sorption. This defines the $\%_{gas\_excluded}$ as:

$$\%_{gas\_excluded} = \frac{\left(n_{gas\_\max} - n_{gas}\right)}{\sum_{all\ gases}\left(n_{gas\_\max} - n_{gas}\right)} \times 100 \tag{19}$$

All these parameters are provided in Table 1.

Table 1: GCMC results using either conditions (i) with the solubilities of all the other penetrants in the polymer phase being artificially set to zero or (ii) with all interactions re-switched on and averaged over 20 GCMC-MD converged configurations at 40 and 60 bar. n_{gas} is the actual number of sorbed gas molecules in the matrix, n_{gas_max} is the maximum number possible in the absence of any interference from the other gases and the $\%_{gas\_excluded}$ is calculated from Eq. (19).

p_{mix} / bar	gas	n_{gas} *(ii)*	n_{gas_max} *(i)*	n_{gas}/n_{gas_max}	n_{gas_max} - n_{gas}	$\%_{gas\_excluded}$
binary 2:1 CH_4/N_2 mixture						
40	CH_4	722	820	88%	98	24%
	N_2	152	463	33%	311	76%
60	CH_4	815	943	86%	128	24%
	N_2	182	593	31%	411	76%
ternary 16:8:1 $CH_4/N_2/CO_2$ mixture						
40	CH_4	528	830	64%	302	29%
	N_2	97	451	22%	354	34%
	CO_2	458	837	55%	379	37%
60	CH_4	594	961	62%	367	28%
	N_2	113	577	20%	464	36%
	CO_2	514	987	52%	473	36%

As expected from the limited swelling in both mixtures (Fig. 9), all n_{gas}/n_{gas_max} in Table 1 are rather close (but not identical) to the similarity factors based on the single-gas uptakes (Fig. 12). In the 2:1 binary mixture, the sorption into the matrix of the least soluble and lower partial pressure N_2 is strongly hindered by that of the more soluble and higher partial pressure component CH_4. CH_4 sorbs up to ~90% of its maximum capacity while N_2 only sorbs up to ~30% of its n_{gas_max}. The much stronger reduction in N_2 agrees with the experimental and modelling observations that the gas whose solubility is less under single-gas conditions exhibits a higher reduction in the mixture [9,

26]. This also translates into the amount of gas molecules excluded from sorbing because of competition. The last two columns of Table 1 show that, for this 2:1 binary mixture, 3/4 of the excluded molecules are N_2 and only 1/4 are CH_4.

In the 16:8:1 ternary mixture, similar trends are seen for CH_4 and N_2, albeit stronger. The added CO_2 contributes significantly to the competitive sorption, even in the absence of plasticization [10]. In spite of its much lower partial pressure, it further reduces the uptakes of both CH_4 and N_2 to ~65% and ~20% of their maximum possible values, respectively, while attaining ~55% of its own. Although this observation has to be treated with caution as its partial pressure interval is limited, a similar order of magnitude for the sorbed CO_2 concentration has been reported experimentally for binary CO_2/CH_4 mixtures in 6FDA-mPDA, PIM-1 or TZ-PIM when CO_2 is at ~10 mol% [8, 11, 13]. On the other hand, in equimolar binary mixtures, CO_2 tends to sorb up to 90-100% of its single-gas capacity when paired with N_2 or CH_4 because of its much higher solubility [10, 20, 21, 26]. In terms of molecules excluded from sorbing because of competition, the actual number of excluded N_2 is not very different from that in the binary mixture as it sorbs little in the first place when paired with CH_4. On the other hand, CH_4 which sorbs easily in the binary mixture is significantly affected by the higher-solubility CO_2. There is also a non-negligible number of excluded CO_2 molecules, but this is probably more because of its relatively low partial pressure than because of its inability to sorb. As a result, the $\%_{gas\_excluded}$ in the 16:8:1 ternary mix are ~28% for CH_4 and ~36% for both N_2 and CO_2. It should be emphasized that the results presented in Table 1 are specific to the composition of the mixtures under study. This approach would warrant testing on many different mixture compositions at a range of conditions, but this is beyond the scope of the present work.

As noted before, the experimental mixed-gas separation factors can be quite different from those obtained from the ideal single-gas values because of those interference effects [9, 94, 119]. The actual sorption selectivities are defined from the concentrations and the partial pressures of the various gases as:

$$\alpha_{A/B}^{S*}(p_{mix}) = \frac{S_A(p_{mix})}{S_B(p_{mix})} = \frac{C_{pol-gasA}(p_{mix})/p_A}{C_{pol-gasB}(p_{mix})/p_B} \tag{20}$$

Fig. 13a shows the mixed-gas CH_4/N_2 sorption selectivities along with those obtained from the DMS mixed-gas predictions as applied to the binary model (Fig. 8a) and the available experimental data [53, 58]. Fig. 13b displays the CH_4/N_2, CO_2/CH_4 and CO_2/N_2 selectivities in the ternary system. All model selectivities are found to be almost pressure-independent, which confirms that, at constant composition, the relative concentration ratios remain the same. Mixed-gas selectivities are indeed known to exhibit a much lower dependence upon pressure than ideal selectivities [9, 14, 20].

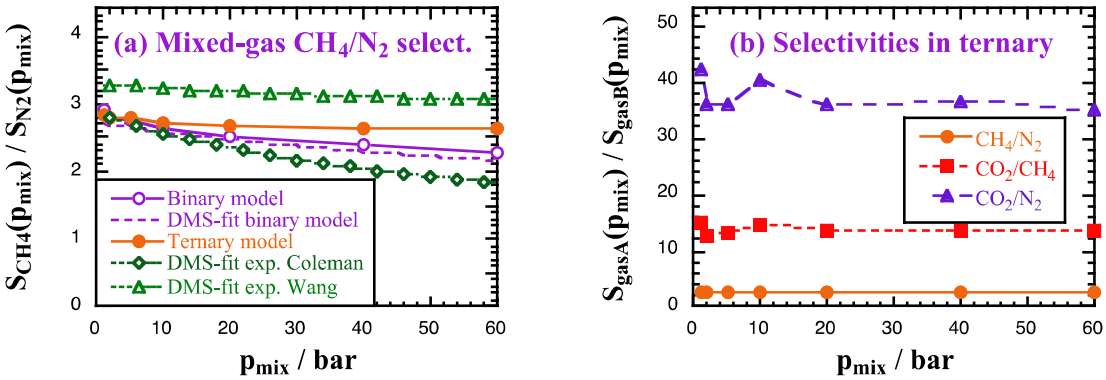

Fig. 13. A comparison of mixed-gas sorption selectivities in 6FDA-6FpDA as function of p_{mix} for **(a)** the CH_4/N_2 pair. The circles are the GCMC-MD data, and the dashed purple line is the mixed-gas DMS prediction as applied to the binary model. The green lines are the mixed-gas DMS predictions using parameters from the fits to the single-gas experimental data of Coleman et al. (diamonds) and Wang et al. (triangles) [53, 58]. **(b)** all three CH_4/N_2, CO_2/CH_4 and CO_2/N_2 pairs in the ternary GCMC-MD model.

Under 2:1 binary conditions (Fig. 13a), the CH_4/N_2 ideal sorption selectivity (Fig. 6a) increases by a factor of ~2 due to the stronger decrease of N_2 sorption with respect to CH_4. At equivalent relative compositions for CH_4 and N_2, the enhancement is only slightly better for the ternary mixture. The model results fall just in between the binary curves predicted from single-gas experiments [53, 58]. Both the latter illustrate the variations that can be obtained in experimental characterizations of the same polymer due to the film-processing procedures and measurement protocols. In spite of their simplifications, model selectivities do compare very well with those expected from experimental sources.

In the 16:8:1 $CH_4/N_2/CO_2$ ternary model (Fig. 13b), the CO_2/CH_4 and CO_2/N_2 real selectivities increase by factors of up to ~5 and to ~10 with respect to their ideal values, respectively. CO_2 decreases considerably the N_2 similarity factor. Indeed, at equimolar

compositions, the sorption of CO_2 hardly deviates from its single-gas isotherm while there is almost no N_2 sorbed [23, 26]. On the other hand, CH_4 is a bit more efficient at competing with CO_2, and as such, the increase in sorption selectivity is not as high [20, 26]. Our CO_2/CH_4 solubility selectivity of ~10 is almost identical to that found experimentally by Genduso et al. for CO_2 at a partial pressure of 2 atm in the 6FDA-mPDA polyimide [11].

These results confirm that, as soon as interference occurs between the various penetrants, single-gas studies combined with the DMS theory clearly have difficulties predicting correctly the actual mixed-gas sorption selectivities. As such, material design based on pure-gas selectivities can be misleading [13, 20] and, whenever possible, new membranes for gas separations should preferentially be tested under mixed-gas conditions.

4. CONCLUSIONS

Three molecular simulation techniques to predict the gas sorption isotherms in a glassy polymer in contact with a single-gas or mixed-gas reservoir of fixed composition have been tested on a ~50000 atom model of the 6FDA-6FpDA polyimide over a wide range of pressures. The gases under study were the low-solubility/non-plasticizing N_2, the medium-solubility/mildly-plasticizing CH_4 and the high-solubility/highly-plasticizing CO_2. In polymer bulk models, there is no explicit contact with the external gas reservoir, and it is necessary to find the conditions under which the chemical potentials of each component are the same in the two phases. The GCMC was unable to take into account the penetrant-induced changes in the polymer matrix, but the TPI-MD and GCMC-MD techniques were more adapted to the task. Both these methods are iterative in the sense that the process has to be repeated until convergence. Their target is to satisfy the equilibrium of the solubility and concentration ratio (Eq. (6)) either by adjusting the pressure (*p*-TPI-MD) or by adjusting the number of penetrants in the polymer matrix (GCMC-MD and *n*-TPI-MD). The excluded volume map sampling approach (EVMS) was successfully incorporated into the GCMC method. Screening out polymer regions of very low insertion probabilities led to improved sampling efficiencies of ~10-20 compared to random insertions.

The single-gas sorption isotherms of CH_4, N_2 and CO_2 in the 6FDA-6FpDA matrix were modelled, and as expected, the uptakes were proportional to the solubilities, *i.e.* $N_2 < CH_4 < CO_2$.

The pressure-iterating *p*-TPI-MD and the GCMC-MD model results compared favourably to experiment and they were able to predict efficiently the ideal sorption selectivities in the glassy matrix.

The iterative methods were further used to model mixed-gas sorption. Test cases were two mixtures consistent with the composition of natural gas, *i.e.* a binary 2:1 CH_4/N_2 and a ternary 16:8:1 $CH_4/N_2/CO_2$ reservoir. In this case, the TPI-MD method had to iterate the numbers of each type of penetrant molecule in the polymer phase instead of the applied pressure. The complexity of adapting this *n*-TPI-MD method meant that it was only applied to the binary mixture. On the other hand, the iterative GCMC-MD method was more easily adaptable to mixed-gas feeds, and it was applied to both the binary and ternary mixtures. Within statistical errors, it gave identical results to the *n*-TPI-MD approach for the binary mixture.

Mixed-gas conditions affected the uptake of each type of penetrant although their normalized solubilities in the polymer phase were very similar as a function of the total penetrant concentration. Indeed, each of the gases under study appeared to occlude a similar quantity of the available space to itself and to the others. On the other hand, the actual concentration of each gas at a given pressure p_{mix} is linked to its partial pressure and to its solubility in both the mixture and polymer phases. For the 2:1 CH_4/N_2 binary mixture, the sorption of the least soluble and lower partial pressure N_2 was hindered by that of the more soluble and higher partial pressure CH_4. As such, the CH_4/N_2 sorption selectivities improved with respect to the ideal values, in agreement with the predictions based on experimental single-gas data. For the 16:8:1 $CH_4/N_2/CO_2$ ternary mixture, the introduction of the highly-soluble CO_2 at a small partial pressure had a significant effect on lowering the uptake of both other penetrants, even if it was not sufficient to really plasticize the polymer. There again, the CH_4/N_2 and CO_2/CH_4 and CH_4/N_2 sorption selectivities differed significantly from their ideal values. A novel procedure was introduced to characterize interference effects by estimating the proportions of molecules of each type of penetrant excluded by competitive sorption. The approach is promising but it requires further testing on different mixture compositions so as to draw general conclusions.

The iterative TPI-MD and GCMC-MD molecular simulation methods implicitly take into account the interdependence of the gas concentrations, solubilities, volume changes and local

relaxation of the polymer. As such, they can be used to assess directly mixed-gas selectivities without the need for single-gas uptake curves. They also allow for the study of sorption over extended pressure and temperature ranges without the difficulties associated with mixed-gas experimental characterizations [11]. In terms of computational efficiency, both types of iterative approaches are relatively close. The MD step is essentially the same for the same period of relaxation and the post-analyses of the stored configurations largely depend on the efficiency of the particle-insertion method. Since EVMS is incorporated into both TPI and GCMC, this step is also now similar in terms of computational time for the same number of configurations analysed. However, it is worth noting that the desired pressure range and intervals can be set in advance in the GCMC-MD and the *n*-TPI-MD (unlike in the *p*-TPI-MD), which reduces the number of simulations that have to be performed. Furthermore, GCMC-MD randomizes the penetrant positions and is much simpler to extend to the case of multi-component gases. It should thus be applicable to even more complex mixtures, which is obviously very pertinent with respect to industrial separation applications.

ACKNOWLEDGEMENTS

This work was partly financed by TOTAL SA within the framework of exploratory projects (PEPS) coordinated by TOTAL SA and the "Cellule Energie" of the CNRS. This work had access to the HPC resources of TGCC/CINES/IDRIS under the allocations A003- A005- and A007-095053 made by GENCI, France. The MUST computing centre at the University Savoie Mont Blanc, France, is also acknowledged for the provision of computer time. N. Charvin is thanked for his help with the installation and maintenance of the laboratory local servers.

REFERENCES

[1] Y. Yampolskii, Polymeric gas separation membranes, Macromolecules, 45 (2012) 3298-3311. https://doi.org/10.1021/ma300213b.

[2] M. Galizia, W.S. Chi, Z.P. Smith, T.C. Merkel, R.W. Baker, B.D. Freeman, 50th anniversary perspective: Polymers and mixed matrix membranes for gas and vapor separation: A review and prospective opportunities, Macromolecules, 50 (2017) 7809-7843. https://doi.org/10.1021/acs.macromol.7b01718.

[3] L.M. Robeson, The upper bound revisited, J. Membr. Sci., 320 (2008) 390-400. https://doi.org/10.1016/j.memsci.2008.04.030.

[4] D.R. Paul, The solution-diffusion model for swollen membranes, Sep. Purif. Methods, 5 (1976) 33 - 50. https://doi.org/10.1080/03602547608066047.

[5] J.G. Wijmans, R.W. Baker, The solution-diffusion model: A review, J. Membr. Sci., 107 (1995) 1-21. https://doi.org/10.1016/0376-7388(95)00102-I.
[6] S. Neyertz, D. Brown, Air sorption and separation by polymer films at the molecular level, Macromolecules, 51 (2018) 7077-7092. https://doi.org/10.1021/acs.macromol.8b01423.
[7] G.O. Yahaya, M.S. Qahtani, A.Y. Ammar, A.A. Bahamdan, A.W. Ameen, R.H. Alhajry, M.M. Ben Sultan, F. Hamad, Aromatic block co-polyimide membranes for sour gas feed separations, Chem. Eng. J., 304 (2016) 1020-1030. https://doi.org/10.1016/j.cej.2016.06.076.
[8] O. Vopička, M.G. De Angelis, G.C. Sarti, Mixed gas sorption in glassy polymeric membranes: I. CO_2/CH_4 and n-C_4/CH_4 mixtures sorption in poly(1-trimethylsilyl-1-propyne) (PTMSP), J. Membr. Sci., 449 (2014) 97-108. https://doi.org/10.1016/j.memsci.2013.06.065.
[9] O. Vopička, M.G. De Angelis, N. Du, N. Li, M.D. Guiver, G.C. Sarti, Mixed gas sorption in glassy polymeric membranes: II. CO_2/CH_4 mixtures in a polymer of intrinsic microporosity (PIM-1), J. Membr. Sci., 459 (2014) 264-276. https://doi.org/10.1016/j.memsci.2014.02.003.
[10] K.L. Gleason, Z.P. Smith, Q. Liu, D.R. Paul, B.D. Freeman, Pure- and mixed-gas permeation of CO_2 and CH_4 in thermally rearranged polymers based on 3,3'-dihydroxy-4,4'-diamino-biphenyl (HAB) and 2,2'-bis-(3,4-dicarboxyphenyl) hexafluoropropane dianhydride (6FDA), J. Membr. Sci., 475 (2015) 204-214. https://doi.org/10.1016/j.memsci.2014.10.014.
[11] G. Genduso, B.S. Ghanem, I. Pinnau, Experimental mixed-gas permeability, sorption and diffusion of CO_2-CH_4 mixtures in 6FDA-mPDA polyimide membrane: Unveiling the effect of competitive sorption on permeability selectivity, Membranes, 9 (2019) 10. https://doi.org/10.3390/membranes9010010.
[12] A.E. Gemeda, M.G. De Angelis, N. Du, N. Li, M.D. Guiver, G.C. Sarti, Mixed gas sorption in glassy polymeric membranes. III. CO_2/CH_4 mixtures in a polymer of intrinsic microporosity (PIM-1): Effect of temperature, J. Membr. Sci., 524 (2017) 746-757. https://doi.org/10.1016/j.memsci.2016.11.053.
[13] E. Ricci, A.E. Gemeda, N. Du, N. Li, M.G. De Angelis, M.D. Guiver, G.C. Sarti, Sorption of CO_2/CH_4 mixtures in TZ-PIM, PIM-1 and PTMSP: Experimental data and NELF-model analysis of competitive sorption and selectivity in mixed gases, J. Membr. Sci., 585 (2019) 136-149. https://doi.org/10.1016/j.memsci.2019.05.026.
[14] E. Ricci, M.G. De Angelis, Modelling mixed-gas sorption in glassy polymers for CO_2 removal: A sensitivity analysis of the dual mode sorption model, Membranes, 9 (2019) 8. https://doi.org/10.3390/membranes9010008.
[15] N. Vergadou, D.N. Theodorou, Molecular modeling investigations of sorption and diffusion of small molecules in glassy polymers, Membranes, 9 (2019) 98. https://doi.org/10.3390/membranes9080098.
[16] W.J. Koros, Model for sorption of mixed gases in glassy polymers, J. Polym. Sci., Polym. Phys. Ed., 18 (1980) 981-992. https://doi.org/10.1002/pol.1980.180180506.
[17] W.J. Koros, R.T. Chern, V. Stannett, H.B. Hopfenberg, A model for permeation of mixed gases and vapors in glassy polymers, J. Polym. Sci. : Polym. Phys. Ed., 19 (1981) 1513-1530. https://doi.org/10.1002/pol.1981.180191004.
[18] F. Doghieri, G.C. Sarti, Nonequilibrium lattice fluids: A predictive model for the solubility in glassy polymers, Macromolecules, 29 (1996) 7885-7896. https://doi.org/10.1021/ma951366c.
[19] M. Minelli, S. Campagnoli, M.G. De Angelis, F. Doghieri, G.C. Sarti, Predictive model for the solubility of fluid mixtures in glassy polymers, Macromolecules, 44 (2011) 4852-4862. https://doi.org/10.1021/ma200602d.

[20] E. Ricci, M. Minelli, M.G. De Angelis, A multiscale approach to predict the mixed gas separation performance of glassy polymeric membranes for CO_2 capture: The case of CO_2 /CH_4 mixture in Matrimid®, J. Membr. Sci., 539 (2017) 88-100. https://doi.org/10.1016/j.memsci.2017.05.068.
[21] E. Toni, M. Minelli, G.C. Sarti, A predictive model for the permeability of gas mixtures in glassy polymers, Fluid Phase Equilib., 455 (2018) 54-62. https://doi.org/10.1016/j.fluid.2017.09.025.
[22] M. Minelli, G.C. Sarti, 110th anniversary: Gas and vapor sorption in glassy polymeric membranes - Critical review of different physical and mathematical models, Ind. Eng. Chem. Res., 59 (2020) 341-365. https://doi.org/10.1021/acs.iecr.9b05453.
[23] C. Rizzuto, A. Caravella, A. Brunetti, C.H. Park, Y.M. Lee, E. Drioli, G. Barbieri, E. Tocci, Sorption and diffusion of CO_2/N_2 in gas mixture in thermally-rearranged polymeric membranes: A molecular investigation, J. Membr. Sci., 528 (2017) 135-146. https://doi.org/10.1016/j.memsci.2017.01.025.
[24] M. Lanč, K. Pilnáček, C.R. Mason, P.M. Budd, Y. Rogan, R. Malpass-Evans, M. Carta, B. Comesaña-Gándara, N.B. McKeown, J.C. Jansen, O. Vopička, K. Friess, Gas sorption in polymers of intrinsic microporosity: The difference between solubility coefficients determined via time-lag and direct sorption experiments, J. Membr. Sci., 570-571 (2019) 522-536. https://doi.org/10.1016/j.memsci.2018.10.048.
[25] J.M. Stubbs, B. Chen, J.J. Potoff, J.I. Siepmann, Monte Carlo calculations for the phase equilibria of alkanes, alcohols, water and their mixtures, Fluid Phase Equilib., 183-184 (2001) 301-309. https://doi.org/10.1016/S0378-3812(01)00442-3.
[26] A. Brunetti, E. Tocci, M. Cersocimo, J.S. Kim, W.H. Lee, J.G. Seong, Y.M. Lee, E. Drioli, G. Barbieri, Mutual influence of mixed-gas permeation in thermally rearranged poly(benzoxazole-co-imide) polymer membranes, J. Membr. Sci., 580 (2019) 202-213. https://doi.org/10.1016/j.memsci.2019.01.058.
[27] D. Tang, G. Kupgan, C.M. Colina, Rapid prediction of adsorption isotherms of a diverse range of molecules in hyper-cross-linked polymers, J. Phys. Chem. C, 123 (2019) 17884-17893. https://doi.org/10.1021/acs.jpcc.9b04413.
[28] D.M. Anstine, A.G. Demidov, N.F. Mendez, W.J. Morgan, C.M. Colina, Screening PIM-1 performance as a membrane for binary mixture separation of gaseous organic compounds, J. Membr. Sci., 599 (2020) 117798. https://doi.org/10.1016/j.memsci.2019.117798.
[29] G. Kupgan, A.G. Demidov, C.M. Colina, Plasticization behavior in polymers of intrinsic microporosity (PIM-1): A simulation study from combined Monte Carlo and molecular dynamics, J. Membr. Sci., 565 (2018) 95-103. https://doi.org/10.1016/j.memsci.2018.08.004.
[30] N.F.A. Van der Vegt, W.J. Briels, M. Wessling, H. Strathmann, The sorption induced glass transition in amorphous glassy polymers, J. Chem. Phys., 110 (1999) 11061-11069. https://doi.org/ 10.1063/1.479042.
[31] F. Müller-Plathe, Permeation of polymers. A computational approach., Acta Polym., 45 (1994) 259-293. https://doi.org/10.1002/actp.1994.010450401.
[32] B. Widom, Some topics in theory of fluids, J. Chem. Phys., 39 (1963) 2808-2812. https://doi.org/10.1063/1.1734110.
[33] S. Pandiyan, D. Brown, S. Neyertz, N.F.A. Van der Vegt, Carbon dioxide solubility in three fluorinated polyimides studied by molecular dynamics simulations, Macromolecules, 43 (2010) 2605-2621. https://doi.org/10.1021/ma902507d.
[34] I. Tanis, D. Brown, S. Neyertz, R. Heck, R. Mercier, M. Vaidya, J.-P. Ballaguet, A comparison of pure and mixed-gas permeation of nitrogen and methane in 6FDA-based polyimides as studied by molecular dynamics simulations, Comp. Mater. Sci., 141 (2018) 243-253. https://doi.org/DOI: 10.1016/j.commatsci.2017.09.028.

[35] D. Brown, S. Neyertz, M.J.T. Raaijmakers, N.E. Benes, Sorption and permeation of gases in hyper-cross-linked hybrid poly(poss-imide) networks: An in silico study, J. Membr. Sci., 577 (2019) 113-119. https://doi.org/10.1016/j.memsci.2019.01.039.
[36] R.W. Baker, Membrane technology and applications, second edition, John Wiley & Sons, Ltd, Chichester, UK., 2004.
[37] T. Spyriouni, G.C. Boulougouris, D.N. Theodorou, Prediction of sorption of CO_2 in glassy atactic polystyrene at elevated pressures through a new computational scheme, Macromolecules, 42 (2009) 1759-1769. https://doi.org/10.1021/ma8015294.
[38] A. Abedini, E. Crabtree, J.E. Bara, C.H. Turner, Molecular simulation of ionic polyimides and composites with ionic liquids as gas-separation membranes, Langmuir, 33 (2017) 11377-11389. https://doi.org/10.1021/acs.langmuir.7b01977.
[39] S. Velioglu, M.G. Ahunbay, S.B. Tantekin-Ersolmaz, Investigation of CO_2-induced plasticization in fluorinated polyimide membranes via molecular simulation, J. Membr. Sci., 417-418 (2012) 217-227. https://doi.org/10.1016/j.memsci.2012.06.043.
[40] S. Velioglu, M.G. Ahunbay, S.B. Tantekin-Ersolmaz, An atomistic insight on CO_2 plasticization resistance of thermally rearranged 6FDA-bisAPAF, J. Membr. Sci., 556 (2018) 23-33. https://doi.org/10.1016/j.memsci.2018.03.047.
[41] M. Balçik, M.G. Ahunbay, Prediction of CO_2-induced plasticization pressure in polyimides via atomistic simulations, J. Membr. Sci., 547 (2018) 146-155. https://doi.org/10.1016/j.memsci.2017.10.038.
[42] R.C. Dutta, S.K. Bhatia, Atomistic investigation of mixed-gas separation in a fluorinated polyimide membrane, ACS Appl. Polym. Mater., 1 (2019) 1359-1371. https://doi.org/10.1021/acsapm.9b00146.
[43] S. Neyertz, D. Brown, Influence of system size in molecular dynamics simulations of gas permeation in glassy polymers, Macromolecules, 37 (2004) 10109-10122. https://doi.org/10.1021/ma048500q.
[44] D. Frenkel, B. Smit, Understanding molecular simulation: From algorithms to applications, 2nd ed., Academic Press, San Diego, CA and London, 2002.
[45] S.V. Lyulin, S.V. Larin, A.A. Gurtovenko, V.M. Nazarychev, S.G. Falkovich, V.E. Yudin, V.M. Svetlichnyi, I.V. Gofman, A.V. Lyulin, Thermal properties of bulk polyimides: Insights from computer modeling versus experiment, Soft Matter, 10 (2014) 1224-1232. https://doi.org/10.1039/c3sm52521j.
[46] S.G. Falkovich, S.V. Lyulin, V.M. Nazarychev, S.V. Larin, A.A. Gurtovenko, N.V. Lukasheva, A.V. Lyulin, Influence of the electrostatic interactions on the thermophysical properties of polyimides: Molecular-dynamics simulations, J. Polym. Sci., Part B: Polym. Phys., 52 (2014) 640-646. https://doi.org/10.1002/polb.23460.
[47] G.L. Deitrick, L.E. Scriven, H.T. Davis, Efficient molecular simulation of chemical potentials, J. Chem. Phys., 90 (1989) 2370-2385. https://doi.org/10.1063/1.455979.
[48] Y. Tamai, H. Tanaka, K. Nakanishi, Molecular simulation of permeation of small penetrants through membranes. 2. Solubilities, Macromolecules, 28 (1995) 2544-2554. https://doi.org/10.1021/ma00111a058.
[49] G. Dömötör, R. Hentschke, Atomistically modeling the chemical potential of small molecules in dense systems, J. Phys. Chem. B, 108 (2004) 2413-2417. https://doi.org/10.1021/jp0367427.
[50] M.R. Coleman, W.J. Koros, Isomeric polyimides based on fluorinated dianhydrides and diamines for gas separation applications, J. Membr. Sci., 50 (1990) 285-297. https://doi.org/10.1016/S0376-7388(00)80626-2.
[51] K. Tanaka, H. Kita, M. Okano, K.-I. Okamoto, Permeability and permselectivity of gases in fluorinated and non-fluorinated polyimides, Polymer, 33 (1992) 585-592. https://doi.org/10.1016/0032-3861(92)90736-G.

[52] K. Matsumoto, P. Xu, T. Nishikimi, Gas permeation of aromatic polyimides. I. Relationship between gas permeabilities and dielectric constants, J. Membr. Sci., 81 (1993) 15-22. https://doi.org/10.1016/0376-7388(93)85027-T.
[53] M.R. Coleman, Isomers of fluorine-containing polyimides for gas separation membranes, Ph.D. Thesis, University of Texas, Austin, TX, 1992.
[54] K. Matsumoto, P. Xu, Gas permeation of aromatic polyimides. II. Influence of chemical structure, J. Membr. Sci., 81 (1993) 23-30. https://doi.org/10.1016/0376-7388(93)85028-U.
[55] M.R. Coleman, W.J. Koros, The transport properties of polyimide isomers containing hexafluoroisopropylidene in the diamine residue, J. Polym. Sci., Part B: Polym. Phys., 32 (1994) 1915-1926. https://doi.org/10.1002/polb.1994.090321109.
[56] M. Mikawa, S. Nagaoka, H. Kawakami, Gas transport properties and molecular motions of 6FDA copolyimides, J. Membr. Sci., 163 (1999) 167-176. https://doi.org/10.1016/S0376-7388(99)00165-9.
[57] K. Tanaka, T. Kawai, H. Kita, K.-I. Okamoto, Y. Ito, Correlation between gas diffusion coefficient and positron annihilation lifetime in polymers with rigid polymer chains, Macromolecules, 33 (2000) 5513-5517. https://doi.org/10.1021/ma992051q.
[58] R. Wang, C. Cao, T.-S. Chung, A critical review on diffusivity and the characterization of diffusivity of 6FDA-6FpDA polyimide membranes for gas separation, J. Membr. Sci., 198 (2002) 259-271. https://doi.org/10.1016/S0376-7388(01)00665-2.
[59] C.J. Cornelius, E. Marand, Hybrid silica-polyimide composite membranes: Gas transport properties, J. Membr. Sci., 202 (2002) 97-118. https://doi.org/10.1016/S0376-7388(01)00734-7.
[60] H. Kawakami, K. Nakajima, H. Shimizu, S. Nagaoka, Gas permeation stability of asymmetric polyimide membrane with thin skin layer: Effect of polyimide structure, J. Membr. Sci., 212 (2003) 195-203. https://doi.org/10.1016/S0376-7388(02)00499-4.
[61] J.H. Kim, W.J. Koros, D.R. Paul, Physical aging of thin 6FDA-based polyimide membranes containing carboxyl acid groups. Part I. Transport properties, Polymer, 47 (2006) 3094-3103. https://doi.org/10.1016/j.polymer.2006.02.083.
[62] R. Recio, L. Palacio, P. Pradanos, A. Hernandez, A.E. Lozano, A. Marcos, J.G. De la Campa, J. De Abajo, Gas separation of 6FDA-6FpDA membranes. Effect of the solvent on polymer surfaces and permselectivity, J. Membr. Sci., 293 (2007) 22-28. https://doi.org/10.1016/j.memsci.2007.01.022.
[63] H. Im, H. Kim, C.K. Kim, J. Kim, Enhancement of gas selectivities of hexafluoroisopropylidene-based polyimides with poly(methylmethacrylate) blending, Ind. Eng. Chem. Res., 48 (2009) 8663-8669. https://doi.org/10.1021/ie900643p.
[64] A. Tena, D. Shishatskiy, D. Meis, J. Wind, V. Filiz, V. Abetz, Influence of the composition and imidization route on the chain packing and gas separation properties of fluorinated copolyimides, Macromolecules, 50 (2017) 5839-5849. https://doi.org/10.1021/acs.macromol.7b01051.
[65] S. Faramawy, T. Zaki, A.A.-E. Sakr, Natural gas origin, composition, and processing: A review, J. Natural Gas Sci. Eng., 34 (2016) 34-54. https://doi.org/10.1016/j.jngse.2016.06.030.
[66] S. Pandiyan, D. Brown, N.F.A. Van der Vegt, S. Neyertz, Atomistic models of three fluorinated polyimides in the amorphous state, J. Polym. Sci., Part B: Polym. Phys., 47 (2009) 1166-1180. https://doi.org/10.1002/polb.21717.
[67] S. Neyertz, D. Brown, S. Pandiyan, N.F.A. Van der Vegt, Carbon dioxide diffusion and plasticization in fluorinated polyimides, Macromolecules, 43 (2010) 7813-7827. https://doi.org/10.1021/ma1010205.
[68] E. Pinel, C. Bas, S. Neyertz, N.D. Albérola, R. Petiaud, R. Mercier, Copolyimides with trifluoromethyl or methoxy substituents. NMR characterization, Polymer, 43 (2002) 1983-1992. https://doi.org/10.1016/S0032-3861(02)00004-6.

[69] D. Brown, *The gmq User Manual Version 5*: available at http://www.lmops.univ-savoie.fr/brown/gmq.html, (2013).
[70] D. Brown, H. Minoux, B. Maigret, A domain decomposition parallel processing algorithm for molecular dynamics simulations of systems of arbitrary connectivity, Comput. Phys. Commun., 103 (1997) 170-186. https://doi.org/10.1016/S0010-4655(97)00040-4.
[71] K.D. Hammonds, J.-P. Ryckaert, On the convergence of the SHAKE algorithm, Comput. Phys. Commun., 62 (1991) 336-351. https://doi.org/10.1016/0010-4655(91)90105-T.
[72] G. Ciccotti, M. Ferrario, J.P. Ryckaert, Molecular dynamics of rigid systems in cartesian coordinates. A general formulation, Mol. Phys., 47 (1982) 1253 - 1264. https://doi.org/10.1080/00268978200100942.
[73] P.P. Ewald, Die Berechnung Optischer und Elektrostatisher Gitterpotentiale, Ann. Phys., 369 (1921) 253-287. https://doi.org/10.1002/andp.19213690304.
[74] S. Neyertz, Tutorial: Molecular dynamics simulations of microstructure and transport phenomena in glassy polymers, Soft Mater., 4 (2007) 15-83. https://doi.org/10.1080/15394450601155608.
[75] S. Neyertz, D. Brown, Preparation of bulk melt chain configurations of polycyclic polymers, J. Chem. Phys., 115 (2001) 708-717. https://doi.org/10.1063/1.1379073.
[76] M. Lal, Monte Carlo computer simulation of chain molecules. I, Mol. Phys., 17 (1969) 57-64. https://doi.org/10.1080/00268976900100781.
[77] H.J.C. Berendsen, J.P.M. Postma, W.F. Van Gunsteren, A. DiNola, J.R. Haak, Molecular dynamics with coupling to an external bath, J. Chem. Phys., 81 (1984) 3684-3690. https://doi.org/10.1063/1.448118.
[78] D. Brown, J.H.R. Clarke, A loose-coupling constant pressure molecular dynamics algorithm for use in the modelling of polymer materials, Comput. Phys. Commun., 62 (1991) 360-369. https://doi.org/10.1016/0010-4655(91)90107-V.
[79] V.M. Nazarychev, A.V. Lyulin, S.V. Larin, A.A. Gurtovenko, J.M. Kenny, S.V. Lyulin, Molecular dynamics simulations of uniaxial deformation of thermoplastic polyimides, Soft Matter, 12 (2016) 3972-3981. https://doi.org/10.1039/C6SM00230G.
[80] S. Neyertz, D. Brown, An optimized fully-atomistic procedure to generate glassy polymer films for molecular dynamics simulations, Comput. Mater. Sci., 174 (2020) 109499. https://doi.org/10.1016/j.commatsci.2019.109499.
[81] W. Humphrey, A. Dalke, K. Schulten, VMD: Visual Molecular Dynamics, J. Mol. Graphics, 14 (1996) 33-38. https://doi.org/10.1016/0263-7855(96)00018-5.
[82] G.C. Boulougouris, I.G. Economou, D.N. Theodorou, On the calculation of the chemical potential using the particle deletion scheme, Mol. Phys., 96 (1999) 905-913. https://doi.org/10.1080/00268979909483030.
[83] G.C. Boulougouris, I.G. Economou, D.N. Theodorou, Calculation of the chemical potential of chain molecules using the staged particle deletion scheme J. Chem. Phys., 115 (2001) 8231-8237. https://doi.org/10.1063/1.1405849.
[84] A. Ben-Naim, Y. Marcus, Solvation thermodynamics of nonionic solutes J. Chem. Phys., 81 (1984) 2016-2027. https://doi.org/https://doi.org/10.1063/1.447824.
[85] J. Vrabec, J. Stoll, H. Hasse, A set of molecular models for symmetric quadrupolar fluids, J. Phys. Chem. B, 105 (2001) 12126-12133. https://doi.org/10.1021/jp012542o.
[86] D. Yin, A.D. MacKerell Jr., Combined ab initio/empirical approach for optimization of Lennard–Jones parameters, J. Comput. Chem., 19 (1998) 334-348. https://doi.org/10.1002/(SICI)1096-987X(199802)19:3%3C334::AID-JCC7%3E3.0.CO;2-U.
[87] Z. Zhang, Z. Duan, An optimized molecular potential for carbon dioxide, J. Chem. Phys., 122 (2005) 214507. https://doi.org/10.1063/1.1924700.
[88] D.J. Tildesley, P. Madden, An effective pair potential for liquid carbon disulphide, Mol. Phys., 42 (1981) 1137-1156. https://doi.org/10.1080/00268978100100861.

[89] M.P. Allen, D.J. Tildesley, Computer simulation of liquids, Clarendon Press, Oxford, UK, 1987.
[90] M.D. Donohue, G.L. Aranovich, Classification of Gibbs adsorption isotherms, Adv. Colloid Interface Sci., 76-77 (1998) 137-152. https://doi.org/10.1016/S0001-8686(98)00044-X.
[91] D.R. Paul, Gas sorption and transport in glassy polymers, Ber. Bunsen-Ges., 83 (1979) 294-302. https://doi.org/10.1002/bbpc.19790830403.
[92] L.M. Robeson, Z.P. Smith, B.D. Freeman, D.R. Paul, Contributions of diffusion and solubility selectivity to the upper bound analysis for glassy gas separation membranes, J. Membr. Sci., 453 (2014) 71-83. https://doi.org/10.1016/j.memsci.2013.10.066.
[93] S. Neyertz, Gas transport in dense polymeric membranes, molecular dynamics simulations, in: E.M.V. Hoek, V.V. Tarabara (Eds.) Encyclopedia of membrane science and technology, John Wiley & Sons, Hoboken, NJ, 2013.
[94] Y. Yampolskii, I. Pinnau, B.D. Freeman, Materials science of membranes for gas and vapor separation, John Wiley & Sons Ltd., Chichester, UK, 2006.
[95] K.C. O'Brien, W.J. Koros, G.R. Husk, Influence of casting and curing conditions on gas sorption and transport in polyimide films, Polym. Eng. Sci., 27 (1987) 211-217. https://doi.org/10.1002/pen.760270306.
[96] G. Mensitieri, M.A. Del Nobile, T. Monetta, L. Nicodemo, F. Bellucci, The effect of film thickness on oxygen sorption and transport in dry and water-saturated Kapton polyimide, J. Membr. Sci., 89 (1994) 131-141. https://doi.org/10.1016/0376-7388(93)E0209-3.
[97] L. Ansaloni, M. Minelli, M. Giacinti Baschetti, G.C. Sarti, Effects of thermal treatment and physical aging on the gas transport properties in Matrimid®, Oil & Gas Science and Technology - Rev. IFP Energies Nouvelles, 70 (2015) 367-379. https://doi.org/10.2516/ogst/2013188.
[98] M. Böhning, J. Springer, Sorptive dilation and relaxational processes in glassy polymer/gas systems - I. Poly(sulfone) and poly(ether sulfone), Polymer, 39 (1998) 5183-5195. https://doi.org/10.1016/S0032-3861(97)10114-8.
[99] J.H. Kim, W.J. Koros, D.R. Paul, Effects of CO_2 exposure and physical aging on the gas permeability of thin 6FDA-based polyimide membranes part 1. Without crosslinking, J. Membr. Sci., 282 (2006) 21-31. https://doi.org/10.1016/j.memsci.2006.05.004.
[100] N.R. Horn, D.R. Paul, Carbon dioxide sorption and plasticization of thin glassy polymer films tracked by optical methods, Macromolecules, 45 (2012) 2820-2834. https://doi.org/10.1021/ma300177k.
[101] M. Wessling, I. Huisman, T. Van der Boomgaard, C.A. Smolders, Dilation kinetics of glassy, aromatic polyimides induced by carbon dioxide sorption, J. Polym. Sci., Part B: Polym. Phys., 33 (1995) 1371-1384. https://doi.org/10.1002/polb.1995.090330907.
[102] A. Bos, I.G.M. Pünt, M. Wessling, H. Strathmann, CO_2-induced plasticization phenomena in glassy polymers, J. Membr. Sci., 155 (1999) 67-78. https://doi.org/10.1016/S0376-7388(98)00299-3.
[103] A.F. Ismail, W. Lorna, Penetrant-induced plasticization phenomenon in glassy polymers for gas separation membranes, Sep. Purif. Technol., 27 (2002) 173-194. https://doi.org/10.1016/S1383-5866(01)00211-8.
[104] J.D. Wind, S.M. Sirard, D.R. Paul, P.F. Green, K.P. Johnston, W.J. Koros, Carbon dioxide-induced plasticization of polyimide membranes: Pseudo-equilibrium relationships of diffusion, sorption, and swelling, Macromolecules, 36 (2003) 6433-6441. https://doi.org/10.1021/ma0343582.
[105] T. Visser, M. Wessling, When do sorption-induced relaxations in glassy polymers set in?, Macromolecules, 40 (2007) 4992-5000. https://doi.org/10.1021/ma070202g.
[106] W. Ogieglo, H. Wormeester, K.J. Eichhorn, M. Wessling, N.E. Benes, In situ ellipsometry studies on swelling of thin polymer films: A review, Prog. Polym. Sci., 42 (2015) 42-78. https://doi.org/DOI: 10.1016/j.progpolymsci.2014.09.004.

[107] S. Neyertz, D. Brown, Nanosecond-time-scale reversibility of dilation induced by carbon dioxide sorption in glassy polymer membranes, J. Membr. Sci., 520 (2016) 385-399. https://doi.org/10.1016/j.memsci.2016.08.003.
[108] K. Simons, K. Nijmeijer, J. Guilera Sala, H. Van der Werf, N.E. Benes, T.J. Dingemans, M. Wessling, CO_2 sorption and transport behavior of ODPA-based polyetherimide polymer films, Polymer, 51 (2010) 3907-3917. https://doi.org/10.1016/j.polymer.2010.06.031.
[109] L.M. Robeson, B.D. Freeman, D.R. Paul, B.W. Rowe, An empirical correlation of gas permeability and permselectivity in polymers and its theoretical basis, J. Membr. Sci., 341 (2009) 178-185. https://doi.org/10.1016/j.memsci.2009.06.005.
[110] S. Neyertz, D. Brown, Molecular dynamics study of carbon dioxide sorption and plasticization at the interface of a glassy polymer membrane, Macromolecules, 46 (2013) 2433-2449. https://doi.org/10.1021/ma302073u.
[111] S. Neyertz, D. Brown, The effect of structural isomerism on carbon dioxide sorption and plasticization at the interface of a glassy polymer membrane, J. Membr. Sci., 460 (2014) 213-228. https://doi.org/10.1016/j.memsci.2014.03.002.
[112] D.F. Sanders, Z.P. Smith, R. Guo, L.M. Robeson, J.E. McGrath, D.R. Paul, B.D. Freeman, Energy-efficient polymeric gas separation membranes for a sustainable future: A review, Polymer, 54 (2013) 4729-4761. https://doi.org/10.1016/j.polymer.2013.05.075.
[113] A. Ben-Naim, Molecular theory of solutions, Oxford University Press, Oxford, UK, 2006.
[114] K.T. Woo, G. Dong, J. Lee, J.S. Kim, Y.S. Do, W.H. Lee, H.S. Lee, Y.M. Lee, Ternary mixed-gas separation for flue gas CO_2 capture using high performance thermally rearranged (TR) hollow fiber membranes, J. Membr. Sci., 510 (2016) 472-480. https://doi.org/10.1016/j.memsci.2016.03.033.
[115] M. Minelli, G.C. Sarti, Gas permeability in glassy polymers: A thermodynamic approach, J. Membr. Sci., 424 (2016) 44-51. https://doi.org/10.1016/j.fluid.2015.09.027.
[116] M. Minelli, G.C. Sarti, Elementary prediction of gas permeability in glassy polymers, J. Membr. Sci., 521 (2017) 73-83. https://doi.org/10.1016/j.memsci.2016.09.001.
[117] A. Bos, High pressure CO_2/CH_4 separation with glassy polymer membranes - aspects of CO_2-induced plasticization, Ph.D. Thesis, University of Twente, The Netherlands, 1996.
[118] Y. Kamiya, T. Hirose, Y. Naito, K. Mizoguchi, Sorptive dilation of polysulfone and poly(ethylene terephthalate) films by high-pressure carbon dioxide, J. Polym. Sci. Part B: Polym. Phys., 26 (1988) 159-177. https://doi.org/10.1002/polb.1988.090260109.
[119] K.C. O'Brien, W.J. Koros, T.A. Barbari, E.S. Sanders, A new technique for the measurement of multicomponent gas transport through polymeric films, J. Membr. Sci., 29 (1986) 229-238. https://doi.org/10.1016/S0376-7388(00)81262-4.